Rotary kiln process: An overview of physical mechanisms, models and applications

Baby-Jean Robert Mungyeko Bisulandu, Florian Huchet

Rotary kiln process:
An overview of physical mechanisms, models and applications

Baby-Jean Robert MUNGYEKO BISULANDU[a,b,*] and Florian HUCHET[c]

[a] Institut de Recherche Futuris - Futuris Research Institute (InReF), OEFC & Faculté Polytechnique, Université Kongo, B.P. 202 Mbanza-Ngungu, Kongo Central, RD Congo

[b] Institut National du Bâtiment et des Travaux Publics (INBTP), Département de Génie Rural, B.P. 4731 Kinshasa, RD Congo

[c] Univ. Gustave Eiffel, MAST-GPEM, F-44344, Bouguenais, France

* Corresponding author: jr.bisulandu@gmail.com

Accepted author manuscript published in Applied Thermal Engineering, 221(2023)
https://doi.org/10.1016/j.applthermaleng.2022.119637

Abstract

The heat and mass transport occurring through a rotary kiln has many industrial applications, such as organic or mineral materials manufacturing. The originality of this review is to explore the various works that have led to a better understanding of rotary kiln process modeling. The paper also details the set of works carried out on the solid load (granular flow regimes, load profile, mean residence time), heat transport (conduction, convection, radiation exchanges) and thermochemical conversion processes (endo- and exothermic reactions). Beginning with the research conducted on directly heated rotary kilns for cement applications, this review extends the scope of application to other fields, including waste, biomass.

Graphical abstract

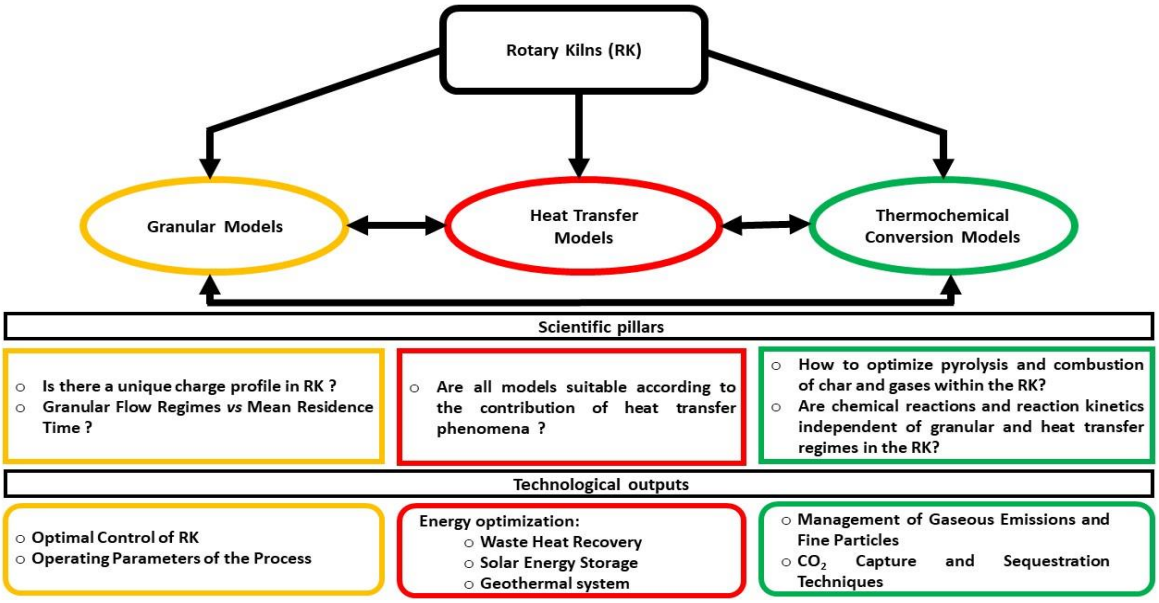

Keywords: Rotary kilns, Granular motion, Heat transfer, Chemical reactions, Kinetics, Modeling

Highlights:

- Solid transport, heat transfer and thermochemical transformation are discussed in detail.
- The heat and mass transfer modeling process in rotary kilns is summarized.
- The commonly used correlations involving rotary kilns are categorized by application.
- The solid-wall heat exchange coefficient is examined.
- The current status, challenges and future direction of this technology are highlighted.

1. Introduction

The rotary kiln is used in many solid processes, including drying, incineration, heating, cooling, humidification, calcination and reduction. This widespread application can be attributed to factors such as the ability to handle varied loads, with large variations in particle size [1]. The rotary kiln is a slightly inclined steel cylinder that rests on supports (bearing rollers) with an interior lining; it is equipped with a rotating motor that induces a turning motion. Such a gas/solid contactor was invented in the cement industry at the beginning of the 19th century. The advent of the rotary kiln is closely tied to the creation of Portland cement. In 1824, Joseph Aspdin successfully produced an eminently hydraulic lime by cooking at high temperature, in a bottle kiln, a mixture of limestone and clays; he referred to his output as "Portland Cement" [2-4]. The bottle kiln however displayed major flaws, among which: it only accepted dry materials; its temperature did not exceed that of the lime kiln; its firing was irregular; it operated only intermittently; and its heating consumed a considerable amount of fuel. In 1872, Johnson came up with the idea of combining the cooking and prior drying of the mixture in an oven, which he called the "chamber kiln or Johnson's kiln" [3]. In 1877, the shaft kiln (a vertical flowing kiln) was invented. This design offered a modification of previous kilns: material and fuel were fed into the kiln from above. The baked clinker flowed out of the bottom. The great revolution in the continuity of the cement production process ultimately stemmed from the commissioning of rotary kilns in 1880 by Thomas Crampton, despite experiencing operational problems [2]. According to Redgrave [3], it was difficult to determine exactly how to improve the operations of rotary kilns, as great uncertainty remained regarding: the exact degree of heat required, the amount of atmospheric air required, the flame effect, the influence of steam, and many other aspects left up to the kiln conductor (employed operator) due to the absence of precisely stated scientific laws. In 1898, Hurry and Seaman improved the design of rotary kilns; they added a cooler to facilitate grinding and improved the quality of the clinker [5]. These improvements thus increased kiln production volumes while yielding a more homogeneous output. Satellite or planetary coolers came into existence in the 1920’s, consisting of a set of tubes (usually 7 to 10) attached to the kiln cylinder [5]. They offer the advantages of being kiln-sealed and not requiring a separate drive. In 1930 in Germany, the first attempts were made to redesign the furnace system in order to minimize fuel waste, which led to two major developments: the grate preheater, and the gas suspension preheater [5]. The advent of preheater ovens also coincided with the appearance of grate coolers, which consist of a perforated grate through which cold air is blown, enclosed in a rectangular chamber. And lastly, kilns equipped with a precalciner were introduced in 1970 in Japan [2,5]; they have since become the equipment of choice for large installations throughout the world. Figure 1 summarizes the various technological advances over the years.

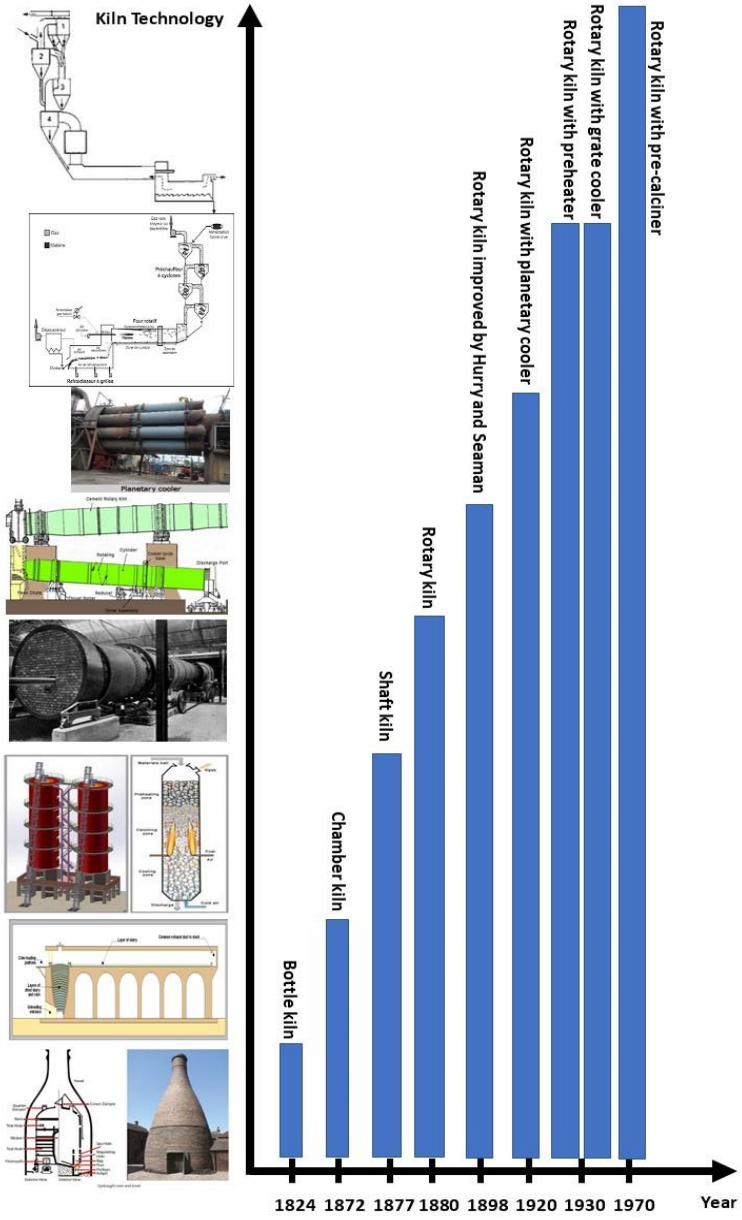

Figure 1: Technological advances of cement kilns over time

This article presents the key stages in the modeling of rotary kilns. First, the parameters characterizing the transport of the solid load are presented in detail. The second part pertains to heat transfer in rotary kilns, featuring a more detailed discussion of heat exchange coefficients. The last part of the article addresses the thermochemical conversion taking place in rotary kilns and provides a broader examination of kiln applications.

2. Solid load transport

The transport of a load into a rotary kiln plays a decisive role in its transformation. Loads may consist of raw materials (raw meal for the cement plant) and/or waste (alternative fuels). In general, the load is introduced counter-currently to hot gases leaving the kiln and generated by a fossil fuel burner; it exits at the other end, after undergoing physicochemical transformations that bring it to the clinker stage. This set-up is specific to cement.

2.1. Transverse behavior

Several authors have focused on the granular motion occurring inside the rotary kiln. Debacq et al. [6] carried out a theoretical and experimental study of the transverse flow of cohesive powders in rotary kilns equipped with lifters. The constitutive law governing the powder discharge, which involves a relationship between the volume fraction of powder contained in a lifter and the angular position of this lifter, was derived and compared with

experimental results. Seidenbecher et al. [7] conducted laboratory-scale experiments on the rotary drum with indirect heating (in discontinuous mode), in order to study grain behavior using various lifter flight designs. Among the different flight length ratios (L_2/L_1) studied, they were able to determine that increasing the flight length ratio to 1 led to improved cooling. The flights used were L-shaped (see Figure 10). For Debacq et al. [6], the rotational speed did not exert any significant influence on either kiln performance or the powders studied. In contrast, Piton et al. [8] stated that the rotational speed considerably influenced the granular mixing regime. Piton et al. [8] developed a one-dimensional thermo-granular model and applied it to an industrial rotary kiln with lifter flights, as characterized by a dense granular regime composed of two passive phases (of the bed and loaded flight) along with a diluted regime characterized by an active phase. The aim of this study was to estimate the surface exchanges between phases that govern heat transfers. Their results showed that an increase in the rotational speed considerably influences the heat transport efficiency.

The geometric parameters related to the transverse behavior in a rotary kiln are given below.
The interception angle of the bed is a key parameter in modeling the solids bed of a rotary kiln. It is defined as the angle subtended by the bed at the center line of the kiln (Figure 2); moreover, it is connected to the transverse cross-section of the bed (A_{bed}) and the inside diameter of the kiln (d_{kiln}) by the following relation (**Erreur ! Source du renvoi introuvable.**) [9,10]:

$$\delta_{bed}(z) - \sin\left(\delta_{bed}(z)\right) = \frac{8 \times A_{bed}(z)}{d_{kiln}^2} \quad (1)$$

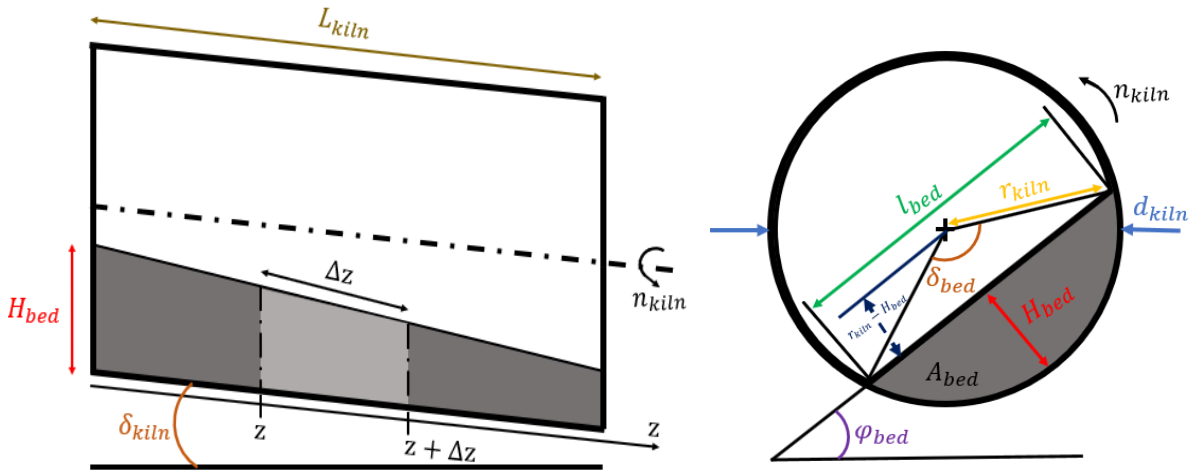

Figure 2: Geometric considerations of the rotary kiln design [11]

The angle of repose is an intrinsic characteristic of a given material; it depends principally on: particle size, rotational speed of the kiln (Figure 2), and surface condition of the kiln wall. More specifically, this angle characterizes the flow properties of "solid particles" in the kiln; it is often assumed to be constant but may vary along the length of the kiln, in correlation with the progress of chemical reactions.

2.1.1. The different types of granular flow regimes

Six material bed movements take place in the transverse plane of the rotary kiln: slipping, slumping, rolling, cascading, cataracting, and centrifuging. Figure 3 illustrates all six of these movements. Boateng and Barr [12] stated that the most desirable bed motion is usually the rolling mode, because it promotes a good mix of particles with a rapid renewal of the bed surface exposed to hot gases flowing into the kiln. Movements such as cascading, cataracting and centrifuging occur at high rotational speeds. Figure 3 summarizes the criteria employed for these different movements.

Basic form	Slipping motion		Cascading ("tumbling") motion			Cataracting motion	
Subtype	Sliding	Surging	Slumping	Rolling	Cascading	Cataracting	Centrifuging
Schematic	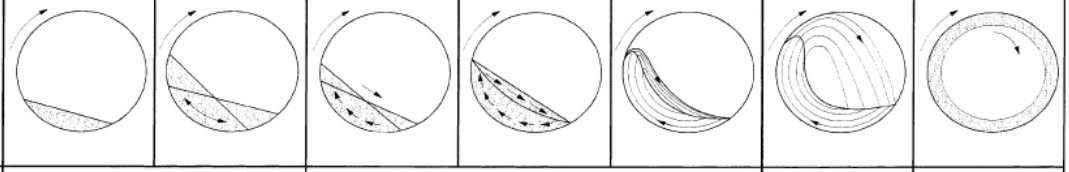						
Physical process	Slipping		Mixing			Crushing	Centrifuging
Froude number Fr [-]	$0 < Fr < 10^{-4}$		$10^{-5} < Fr < 10^{-3}$	$10^{-4} < Fr < 10^{-2}$	$10^{-3} < Fr < 10^{-1}$	$0.1 < Fr < 1$	$Fr \geq 1$
Filling degree f [-]	$f < 0.1$	$f > 0.1$	$f < 0.1$	$f > 0.1$		$f > 0.2$	
Wall friction coeff. μ_w [–]	$\mu_w < \mu_{w,c}$	$\mu_w \geq \mu_{w,c}$	$\mu_w > \mu_{w,c}$			$\mu_w > \mu_{w,c}$	
Application	no use		Rotary kilns and reactors; rotary dryers and coolers; mixing drums			Ball mills	no use

Figure 3: Granular flow regimes and the Froude number associated with each bed movement [13]

Yin et al. [14] stated that the flow into the active layer depends mainly on both the Froude number ($Fr = \omega^2 R/g$, where ω is the angular velocity of rotation and g the acceleration of gravity) and size ratio ($s = d_p/R$, where d_p is the particle diameter and R the radius of the kiln cylinder). Details on the various types of movements can be found in previous works [11–13]. In their work on the slumping-rolling transition of granular solids in rotary kilns, Liu et al. [15] developed a mathematical model to calculate the critical Froude number. Their results showed that the critical Froude number is proportional to the ratio of the particle size to the cylinder diameter (d_p/D) and inversely proportional to $\sin^2(\delta_{bed}/2)$, where δ_{bed} denotes the filling angle of the solid bed.

Eulerian modeling is another technique used to model granular beds in a rotary kiln. Many works from the literature have addressed the Eulerian modeling of granular beds in rotary kilns; in particular, Yin et al. [16] developed a three-dimensional granular model, based on two-phase Euler-Euler flow, for rotary kilns operating in rolling mode, with the aim of determining the speed profiles of particles in the bed material. This model considers the various operating parameters, with emphasis on both the angle of inclination and particle residence time. The output of this model has shown that the active layer thickness and granular particle velocities increase with axial distance. However, the active layer thickness and particle velocities close to the discharge end of the kiln once again decrease. These authors noted the presence of three distinct regions in the rolling mode: the active region, the passive region, and the active-passive interface (as the surface of the bed is not flat and becomes slightly S-shaped). Particles at the bed surface jump in order to move without sliding or rolling. Liu et al. [17] presented a two-dimensional model of a rotary kiln coupled with the kinetic theory of granular flow, in order to treat random granular motion as well as simulate the mixture performance. The effects of rotational speed, particle diameter and bulk gas temperature on temperature distribution were explored. The main objective of their model was to clarify the heat transfer mechanisms coupled with the movement of particles in rotary kilns. As was the case for Yin et al. [16], Liu et al. [17] affirmed that the highest bed temperatures were indeed located at the surface, while the lowest bed temperatures were located in the passive layer.

According to Yin et al. [16], a Discrete Element Modeling (DEM) study is to be conducted to help understand flow processes and explain mixing mechanisms in mixing equipment relying on a rotating drum. Witt et al. [18] developed an approach combining the DEM of bed slices and two-phase computational fluid dynamics (CFD) 3D models of the entire kiln, thus encompassing both the bed and freeboard gaseous edge. The goal therein was to derive the average velocities of solids in a bed for various rotational speeds and particle sizes, so as to calibrate and validate the rheological model of the solid phase. Saruwatari and Nakamura [19] also worked with the DEM method in application to particle behavior. In nearly all the models mentioned above, the rotational speed of the kiln plays a determining role.

2.1.2. Segregation problem

Load transport in rotary kilns is often accompanied by segregation problems. Segregation takes place because the particles are not of either uniform size or uniform density. Shape segregation can also occur. According to Cantelaube et al. [20] and Khan and Morris [21], segregation is a property of dry granular solids, which tend to separate spatially by size, shape or density under varying flow conditions. For Bongo Njeng et al. [22], the segregation phenomenon has been observed in industrial processing involving granular materials; moreover, it has been widely studied within the context of rotating drums. According to Boateng and Barr [1,12], the vigorous mixing of particles and the high renewal rate of particles in the transverse surface of the bed constitute the key features of the active layer. However, since the particles are not always similarly sized, smaller particles often tend to pass through the screen formed by larger particles, which gives rise to the phenomenon called segregation. For Cantelaube et al. [20] and Beaulieu et al. [23] with respect to rolling motion, radial segregation may appear very quickly, causing a concentration of smaller particles toward the core of the bed, while larger particles may roll in the active layer depending on the inclination at the bed surface. This phenomenon is deleterious from the standpoint of both the chemistry and physics of thermochemical particle transformation. During segregation, the finer particles concentrate at the heart of the bed, thus forming a cooling core [12,24]. As such, they have a lower temperature than the surrounding material, since they are unable to reach the bed surface, which is directly exposed to the heat flow stemming from the combustion of gas at the burner [12]. Bongo Njeng et al. [22] investigated the effects of pusher shape and configurations, kiln rotational speed and slope, and mass flow rate on solid particle segregation. They noted the elements that characterize segregation, namely: the broad particle size distribution, involving both larger and smaller particles and heavier and lighter particles, and particle concentration. The results of this study reveal that for higher degrees of filling, the phenomenon of segregation occurs in the transverse plane, between heavier particles and lighter particles.

2.2. Longitudinal behavior

2.2.1. Load height along the rotary kiln

The bed height in a rotary kiln depends on several parameters, including mass loss in the solids bed and the geometric parameters of both the bed and kiln [25,26]. Several models of changes in depth along the kiln have been built. Kramers and Croockewit [26] established a model set up as a differential equation. Wu et al. [27] worked on a pilot rotary kiln with direct heating in order to propose a method that allows automatically measuring the local depth of material in a kiln. From these works, it then follows that the geometric parameters exert great influence on the bed depth determination. This model yields the bed height according to the axial position in the rotary kiln. Mujumdar and Ranade [28] relied on the model proposed by Kramers and Croockewit [26] (see Table 1). In their experimental research on solid bed depth at the discharge end of rotary kilns, Specht et al. [29] proposed a correlation to estimate the bed height (Table 1). Davies et al. [30], Granados et al. [31] and Liu and Specht [32] also presented a relationship to allow estimating bed height along the kiln (Table 1). The correlations proposed in [23, 33-35] have been derived from those in [26, 36, 37]. Knowledge of the bed height thus makes it possible to calculate the degree of filling of the kiln, by means of Equation (2) [25]:

$$f = \frac{1}{2 \times \pi} \times \left(2 \times \cos^{-1}\left(\frac{r_{kiln}}{r_{kiln} - H_{bed}}\right) - \sin\left[2 \times \cos^{-1}\left(\frac{r_{kiln}}{r_{kiln} - H_{bed}}\right)\right]\right) \qquad (2)$$

Colin [38] proposed a relationship for calculating the angle of interception of the bed $\delta_{bed}(z)$, based on knowing the bed height (Table 1). Mungyeko Bisulandu [11] used the work of Mujumdar and Ranade [28], who themselves made use of the correlation found by Kramers and Croockewit [26], and Saeman [36]. In this particular model, the dynamic angle of repose of the bed φ_{bed} is assumed to be constant and equal to its value at the kiln entrance.

2.2.2. Mean Residence Time (MRT) models

MRT is a key parameter for solid load transport modeling in rotary kilns. Many works have dealt with MRT in rotary kilns; notably, Haeldermans et al. [39] developed a model to predict the residence time of solids in a rotary kiln. Their study focused on analyzing the influence of both the kiln's geometric and operating parameters (i.e. rotational speed and inclination) on the mean residence time (MRT). These authors claimed to have tested several models existing in the literature, which yielded poor results, hence their adaptations of the models of Saeman [36], Sullivan et al. [40], Chatterjee et al. [41] and the United States Geological Survey (Green and Perry [42]) produced small errors. Donatelli et al. [43] derived a theoretical approach based on understanding the amount of bed material to be discharged into an inclined rotary kiln (empty cylinder), under conditions akin to a slumping motion and with a known particle size distribution (PSD). The results of this model showed that the larger particles lie ahead of the smaller ones and moreover that residence time depended on the particle diameters. In

general, the MRT correlations depend on three geometric parameters and a maximum of four operating parameters. The models of Sullivan et al. [40], Lee and Lin [44], Chatterjee et al. [41] and Green and Perry [42] are all similar and lead to nearly identical results (Table 1 below).

2.2.3. Analysis of the different load model heights

Despite being expressed in different ways, the various correlations presented above are, in most cases, equivalent and derived from the efforts of the pioneers in this field, namely Kramers and Croockewit [26], Saeman [36] and Vàhl and Kingma [37].

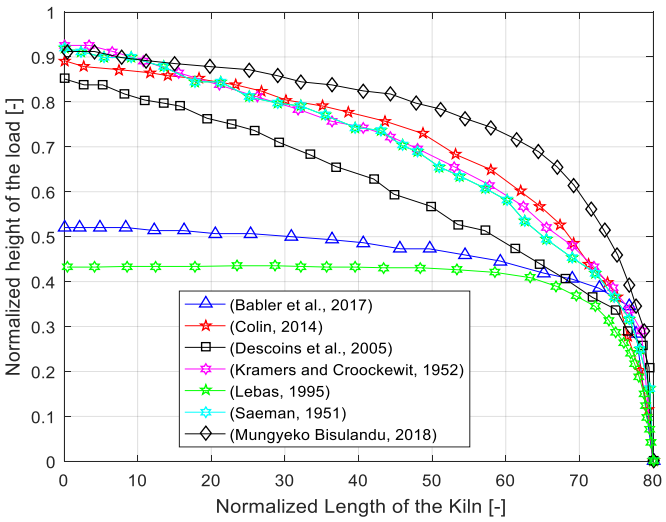

Figure 4: Various models found in the literature

Figure 4 above depicts the load profiles obtained from equations given in seven works from the literature. Despite the differing flow rates at the kiln entrance, these profiles are still comparable because the boundary conditions for solving these correlations are all given at the kiln outlet. The various correlations used in determining the load height are indeed equivalent; they have all been derived from the pioneering work of Saeman [36] and Kramers and Croockewit [26]. Their solution requires boundary conditions at either the rotary kiln entrance or outlet. The outlet condition often receives consideration, in assuming that the outlet load has a height equivalent to that of the diaphragm, or the heel of a grain (clinker, particle, etc.).

Table 1: Granular models found in the literature

Load height models						
Equations	$\frac{dH_{bed}(z)}{dz} = \frac{3 \times tan\,\varphi_{bed}}{4 \times \pi \times kiln} \times q_v \times [R^2 - (H_{bed}(z) - R)^2]^{-3/2} - \frac{tan\,\delta_{kiln}}{cos\,\varphi_{bed}}$	$\frac{dH_{bed}(z)}{dz} = tan\,\varphi_{bed} \times \left[\frac{tan\,\delta_{kiln}}{sin\,\varphi_{bed}} - \frac{3 \times q_v}{4 \times \pi \times n_{kiln} \times r_{kiln}^3} \times \left(\frac{2 \times H_{bed}(z)}{r_{kiln}} - \frac{{H_{bed}}^2(z)}{r_{kiln}^2}\right)^{-3/2}\right]$	$\frac{dH_{bed}(z)}{dz} = \frac{0.75 \times tan\varphi_{bed}}{\pi \times n_{kiln}} \times \frac{q_m}{\rho_s} \times [r_{kiln}^2 - (H_{bed} - r_{kiln})^2]^{-3/2} - \frac{tan\,\delta_{kiln}}{tan\,\varphi_{bed}}$	$\frac{dH_{bed}(z)}{dz} = tg\left[\frac{4 \times q_v \times sin\varphi_{bed}}{0.16661 \times n_{kiln} \times r_{kiln}^3} \times (\delta_{bed} - sin\,\delta_{bed})^{0.75} - \delta_{kiln}\right]$	$\frac{dH_{bed}(z)}{dz} = \frac{tan\varphi_{bed}}{4 \times \pi \times n_{kiln}} \times \left[\frac{q_v}{(r_{kiln}^2 - (H_{bed} - r_{kiln})^2)^{3/2}}\right] - \frac{tan\,\delta_{kiln}}{cos\,\varphi_{bed}}$	$H_{bed}(z) = r_{kiln} \times \left(1 - cos\left(\frac{\delta_{bed}(z)}{2}\right)\right)$
Original Authors	Saeman [36]	Kramers and Croockewit [26] and Saeman [36]	Saeman [36]	Perron and Bui [45]	Scott et al. [46]	Saeman [36], Danish et al.[47]
User Authors	Haeldermans et al. [39] ; Zhang et al.[48] ; Parveen et al.[49]; Ndiaye et al.[50]; Zheng et al. [51];Witt et al. [52]	Mujumdar and Ranade [28], Kramers and Croockewit [26]	Specht et al.[29]	Perron and Bui [45]	Granados et al.[31] , and Liu and Specht [32]	Colin [38]; Gallo et al.[53] ; Ngako et al.[35],Danish et al.[47], Parveen et al.[49];Wu et al.[27]
Application	- Syngas treatment - Solid materials treatment	- Solid materials treatment - Cement production	- Solid materials treatment	- Solid materials treatment - Thermal treatment	- Solid materials treatment	- Thermal treatment - Solid materials treatment - Cement production
Mean Residence Time (MRT)						
Equations	$MRT = 3.80 \times \frac{L}{D} \times \frac{\sqrt{\varphi_{bed}}}{n_{kiln} \times \delta_{kiln}}$	$MRT = 1.77 \times \frac{L}{D} \times \frac{\sqrt{\varphi_{bed}}}{n_{kiln} \times \delta_{kiln}}$	$MRT = \frac{0.1026 \times L^3}{\dot{V}} \times \left(\frac{\varphi_{bed}}{\delta_{kiln}}\right)^{1.054} \times \left(\frac{\dot{V}}{L^3 \times n_{kiln}}\right)^{0.981} \times \left(\frac{L}{D}\right)^{1,1}$	$MRT = 0.19 \times \frac{L}{D} \times \frac{1}{n_{kiln} \times \delta_{kiln}}$	$MRT = \frac{0.23 \times L}{\delta_{kiln} \times n_{kiln}^{0.9} \times D}$	$MRT = \frac{78912 \times h_{bed}^{0.24}}{(tan^{-1}s)^{1.02} \times n_{kiln}^{0.88} \times (\pi \times r^2 \times F)^{0.0072}}$	$MRT = \frac{M_c}{G_c}$
Original Authors	Sullivan et al.[40]	Sullivan et al.[40]	Chatterjee et al.[41]	Lee and Lin [44]	Green et Perry [42]	Cholette and Cloutier [54]	Donatelli et al.[43]
User (Authors)	Haeldermans et al.[39]	Sullivan et al.[40] ; Mintus et al.[55]	Chatterjee et al.[41];Lasek et al. [56]	Ngako et al. l.[35] ; Ndiaye et al. [50]	Green et Perry [42]	Renaud et al.[57], Alonso et al. [58]	Donatelli et al.[43]
Application	- Syngas production	- Solid materials treatment - Cement production	- Iron manufacturing - Thermal treatment	- Solid materials treatment	- Solid materials treatment	- Solid materials treatment - Thermal treatment	- Thermal treatment

Interception angle of the bed					
Equations	$\delta_{bed} = arccos\left[1 - \frac{H_{bed}(z)}{R}\right]$	$\delta_{bed}(z) - sin(\delta_{bed}(z)) = \frac{8 \times A_{bed}(z)}{d_{kiln}^2}$			
Original Authors	Saeman [36]	Marias et al.[10]			
User (Authors)	Haeldermans et al. [39], Descoins et al.[9]	Marias et al.[10], Mungyeko Bisulandu [11]			
Application	- Syngas treatment	- Solid materials treatment - Thermal waste treatment			
Cross-sectional area of the solid bed					
Equations	$A_{bed} = r_{kiln}^2 \times cos^{-1}\left(\frac{r_{kiln} - H_{bed}}{H_{bed}}\right) - (r_{kiln} - H_{bed}) \times (2 \times r_{kiln} \times H_{bed} - H_{bed}^2)^{1/2}$	$A_{bed} = \frac{1}{2} \times \left(\frac{d_{kiln}}{2} \times \delta_{bed}(z) - l_{bed}(z) \times \left(\frac{d_{kiln}}{2} - H_{bed}(z)\right)\right)$	$A_{bed} = \frac{1}{2} \times r_{kiln}^2 \times \left(\delta_{bed}(z) - sin(\delta_{bed}(z))\right)$		
Original Authors	Henein et al. [59]	Mujumdar and Ranade [28]	Saeman [36]		
User (Authors)	Henein et al. [59]	Mujumdar and Ranade [28], Mungyeko Bisulandu [11]	Saeman [36], Descoins et al. [9]		
Application	- Solid materials treatment	- Cement production - Waste treatment	- Solid materials treatment		

2.3. Contribution of advanced numerical methods

Obviously, nearly all granular models of rotary kilns existing in the literature are presented in rolling mode. However, two major schools of thought or philosophies can be identified in terms of granular flow modeling, namely:

- considering the bed of solids as a one-dimensional model, perfectly mixed at each cross-sectional slice, with the bed material being isothermal over the entire cross-section of the kiln (e.g. Mungyeko Bisulandu [11], Marias et al. [10], Mujumdar and Ranade [28]);
- considering the bed as a two-phase (discrete) flow model, either of the Euler-Euler type or the Euler-Lagrange type (e.g. Yin et al. [16], Liu et al. [17], Demagh et al. [60], Orpe and Khakhar [61]), wherein the particle trajectory is followed individually. This type of model aims to understand the flow processes and mixing mechanisms taking place in the rotary kiln.

In both cases, the operating parameters such as the dynamic and static angles of repose of the bed, degree of filling, ratio between particle diameter and kiln, coefficient of wall friction, coefficient of internal friction and rotational speed play a considerable role in characterizing the transverse motion of the bed [13]. Mellmann [13] concluded that the length and inclination of the kiln have no influence on the transverse movement, yet they do essentially determine the axial transport in the kiln. The discrete model seems to be more efficient than the initial model, insofar as it becomes possible to: track the displacement of particles on the surface step-by-step, and understand their behavior at each position of the transverse plane of the bed. According to Yin et al. [16], a complete understanding of surface flows is key to an accurate representation of the entire flow dynamics. Regarding the study of the segregation phenomenon, two key parameters are therefore important, i.e. particle size and density. Segregation can be generated either by a size ratio or by a density ratio. Density segregation is less common than size segregation [59-61].

The experimental proof of such phenomena has been extensively supported by numerical simulations performed with a geometry similar to that found in RK. The literature always shows that radial segregation tends to be more widely observed than axial segregation; moreover, axial transport is strongly favored by continuous flow at the bed surface.

3. Heat transfer in a rotary kiln

Heat transfer plays a critical role in the preparation of clinker for a rotary kiln. Often supplied with energy by means of a burner placed at its end, the rotary kiln is the site of numerous heat transfers between walls, and loads circulating and the gas circulating above the free surface of the bed. As for the granular model, several models have been proposed to predict the thermal behavior of rotary kilns. Heat transfer in the rotary kiln occurs between different components: the solids bed, walls, and gases. Ginsberg and Modigell [65] selected the following heat transfer mechanisms for their model: the transfer between gases, the gas side wall and the solids bed surface; direct heat transfer from gases to the wall occurring by convection and radiation; the radiative flux from the wall to the solids bed; heat transfer between the walls and the solids bed; regenerative heat transfer in the kiln wall; and transfer from the outer shell of the kiln to the environment. Heat transfer in the solids bed is controlled, for example, by granular movement (i.e. solids in the bed). Thornton and Batterham [66], Gorog et al. [67], Thurlby [68] and others have hypothesized that conduction and radiative heat fluxes would be negligible in the axial direction of the kiln. According to Boateng and Barr [1], several models proposed in the literature have sought to assume that the bed in the transverse plane is well mixed at each axial position along the kiln and furthermore that the bed material is isothermal over the entire cross-section of the kiln. In his work, Nielsen [69] asserted that in a cement rotary kiln, it was possible to assume a rapid mass transfer of oxygen in the active layer and a passive layer transfer taking place by means of relatively slow diffusion. In their studies of the heat transfer model in the bed, Boateng and Barr [1] concluded that the ability to simulate freeboard transport phenomena is greater than the ability to accurately determine conditions in the bed. Seidenbecher et al. [7] also worked on heat transfer in the rotary kiln. They took into account the axial, radial and circumferential temperature profiles in different kiln components, namely the gas phase, the solid phase (bed of solid particles) and the kiln wall. They presented the temperature-time profiles and temperature drop as a function of the flight length ratio plus the number of flights. To control the heat transfer in the rotary kiln, Atmaca and Yumrutaş [67, 68] suggested carrying out an exergy analysis, which according to them provides critical information on the design of cost-effective energy systems. Their formulations included: mass, energy and exergy balances; efficiency and specific energy consumption; and cost analyses based on two methods of energy and exergy analysis.

3.1. Heat transfer mechanisms

Heat exchanges in the rotary kiln generally occur in the three conventional modes of heat transfer: conduction, convection, and radiation, as well as between the three constituent elements, namely: the solids bed, the walls, and the gas. The various possible flows are as follows (Figure 5): Gas/Solids exchange by convection $\varphi_{gasFB-B}^{Conv}$ and radiation $\varphi_{gasFB-B}^{Rad}$; Gas/Wall exchange by convection $\varphi_{gasFB-W}^{Conv}$ and radiation $\varphi_{gasFB-W}^{Rad}$; Solids/Wall exchange covered by conduction φ_{wall-B}^{Cond}; Solids/Wall exchange exposed or uncovered by radiation φ_{wall-B}^{Rad}; and Outer Wall/Ambient Air exchange by convection $\varphi_{wall-air}^{Conv}$ and radiation $\varphi_{wall-air}^{Rad}$.

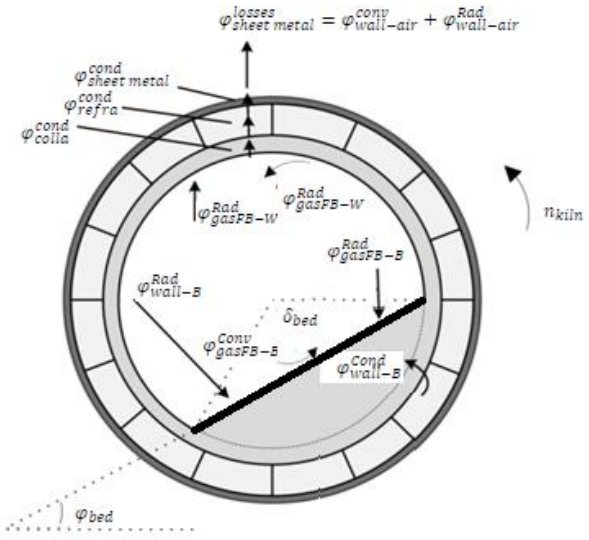

Figure 5: Heat exchanges taking place in a rotary kiln [11]

Wall-to-particle and particle-to-particle transfers are not negligible when calculating the heat balance of a rotary kiln. The wall-to-bed transfer of solids actually takes place between the particle in the bed and the surface of the wall, which are in direct contact (Figure 6). This process characterizes the speed at which heat is transferred step by step, i.e. from wall to particle and then from particle to particle. This transfer is only possible when pairs of particles come into contact with one another. Such a mechanism is entirely conductive. Although wall-to-particle and particle-to-particle transfers constitute two completely different mechanisms, many works from the literature summarize them as wall-to-solid transfers. This codification makes it possible to simplify the system of equations but does not allow for a good representation of reality. The ideal would be to split the wall-to-bed transfer mechanism into two coupled mechanisms. Tsotsas [72] stated that the heating of a particulate material by contact with the hot wall of a rotating drum or the hot bottom of a tray equipment used to mix the particles by a rotating agitator remains an unresolved problem.

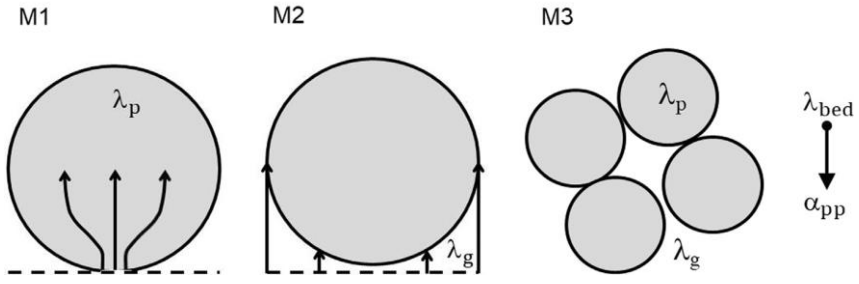

Figure 6: Illustration of the three competing models of particle-to-particle heat transfer [72]

3.1.1. Heat transfer by conduction (Wall-Covered Solid)

This transfer mode is carried out between the solids bed and the covered wall of the rotary kiln. The walls, due to their contact with the gases (exposed gas-wall exchange), heat up and exchange heat with the solids bed

during kiln rotation (the exposed wall becomes the covered wall, and *vice versa*). As this exchange is taking place, the covered wall cools and releases a certain amount of heat previously received from the gas phase. This phenomenon is therefore considered a regeneration (heat transfer from the gas to the load, via the wall) [73]. Several researchers have carried out studies on wall-solid heat transfer by conduction, in particular on the wall-solid exchange coefficient, especially Csernyei and Straatman [74], and Mujumdar and Ranade [28], who used the correlation derived by Tscheng and Watkinson [75]. Ginsberg and Modigell [65] modeled the wall-solid exchange coefficient according to the following relationship (3):

$$\frac{1}{h_{wall-B}} = \frac{1}{(h_{wall-B})_{wall}} + \frac{1}{(h_{wall-B})_{B}} \quad (3)$$

where $(h_{wall-B})_{wall}$ denotes the heat transfer coefficient of contact between the wall and the solid (W/m^2/K), and $(h_{wall-B})_{B}$ the heat transfer coefficient of mass penetration of the solid (W/m^2/K). This last relation represents the placement in series of two resistances of contact $(1/(h_{wall-B})_{wall})$ and penetration $(1/(h_{wall-B})_{B})$. The contact resistance depends on both the thermal conductivity of the gas between particles and the radiative heat transfer between the wall and the solids. According to Ginsberg and Modigell [65], $(h_{wall-B})_{wall}$ remains constant along the kiln, allowing them to use the average value of 377 W/m^2/K. Marias et al. [10] opted for the value of 25 W/m^2/K as the wall-solid exchange coefficient; this value has been adjusted to obtain the ambient temperature for the solid bed at the kiln outlet, whereas E. Mastorakos et al. [76] evaluated the exchange coefficient h_{wall-B} at 500 W/m^2/K, as derived from the results of Barr et al. [77]. Lybaert [78] proposed values of h_{wall-B} lying between 50 and 350 W/m^2/K. Agrawal and Ghoshdastidar [79] modeled the wall-solid transfer in assuming the heat conduction to be quasi-static (since the kiln wall is alternately heated and cooled during each revolution by the gas and solid, respectively). As for the wall-solid exchange coefficient, a value of 377 W/m^2/K was selected, as given by Ginsberg and Modigell [65]. Shi et al. [80] and Specht [81] modeled the exchange coefficient by wall-solid conduction according to the theory of penetration, as offered by the correlation in Table 3. Specht [81] reported the correlation of the direct contact heat transfer coefficient $(h_{wall-B})_{wall}$, as extracted from the work of Sullivan and Sabersky [82] and Li et al. [83]:

$$(h_{wall-B})_{wall} = \frac{1}{\Gamma} \times \frac{\lambda_{gas}}{d_p} \quad (4)$$

with $\Gamma = 0.1$, which is determined experimentally. λ_{gas} is the thermal conductivity of the gas and d_p the mean particle diameter. Figure 7 enables visualizing the heat transfer coefficient, which consists in series of the resistance to direct contact of the first particle layer and resistance to penetration into the other particle layers.

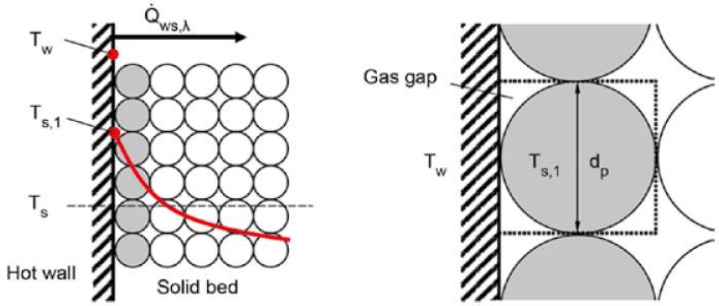

Figure 7: Heat transfer from a hot wall into the bed [81]

Babler et al. [84] used the correlation (Table 2) based on two resistances: resistance to heat transfer caused by the gas film surrounding the particles, and resistance to heat transfer caused by the particle material itself. Wes et al. [85] proposed the correlation in logarithmic form to estimate the wall-solid thermal exchange coefficient. The correlation proposed by Tscheng and Watkinson [75] and used in most research papers (Huchet et al. [86], Piton et al. [87]) is as follows (5):

$$h_{wall-B} = 11.6 \times \frac{\lambda_{bed}}{2 \times \delta_{bed} \times r_{kiln}} \times \left(\frac{2 \times \omega \times r_{kiln}^2 \times \delta_{bed}(z)}{D_{bed}} \right)^{0.3} \quad (5)$$

This relation is only valid for kiln rotational speeds between 3.5 and 10 (rad/s). In their modeling and simulation of the temperature field in the rotary kiln for iron ore, Fan et al. [88] proposed the correlation in Table 2, where δ_{gf} is the thickness of the gas film (m), γ_f the coefficient of adjustment for calculating heat conduction, and t_c the particle-wall contact time (s). Other authors have associated radiation with the wall-solid transfer, while others have mentioned the phenomenon of convection, as observed in the bed pores (with considerable porosity). Lebas [89] took into account the phenomenon of radiation occurring in the interstices between walls and solid particles when calculating the overall covered wall-solid transfer coefficient. In their studies on particle motion and heat transfer in a rotary kiln, Liu et al. [90] proposed the following empirical correlation (combining convection and conduction) to calculate the exchange coefficient between covered wall and solids bed. As stated above, the regenerative heat transfer of the wall serves as a key mechanism in wall-to-solid heat transfer. The overall regenerative heat transfer is composed of the three series-connected heat resistances: gas-wall heat transfer, wall transport, and wall-solid heat transfer [81]. Specht [81] represented the regenerative heat transfer coefficient by:

$$h_{regen} = \frac{1}{\frac{1}{h_{wall-B}} + \frac{1}{h_{trans}} \times \frac{\delta_{bed}}{\pi} + \frac{1}{h_{gasFB-W}} + \frac{\delta_{bed}}{\pi - \delta_{bed}}} \quad (6)$$

where h_{trans} denotes the heat flux transfer coefficient transported to the bed, as given by $h_{trans} = \sqrt{\pi \times \lambda \times \rho \times Cp.n_{kiln}}$ [81]. The correlations presented above all yield results, yet the most comprehensive and realistic is that given by Ginsberg and Modigell [65], who studied two mechanisms in coupled form related to the wall-bed exchange. A third mechanism can however be added to Equation (19), which will account for the radiation effect of gases in the interstices between walls and solid particles, as proposed by Lebas [89].

3.1.2. Heat transfer by convection

In a smooth rotary kiln, convection heat transfer pertains to: gas-solid contact, gas-wall contact, and exterior wall-ambient air contact. When lifters are taken into consideration, the gas-to-free fall grain needs to be accounted for in the heat transfer phenomena.

3.1.2.1. Gas-solid transfer

The gas-solid transfer essentially pertains to the heat flow received by the bed, through its upper surface, in direct contact with the gas phase. As regards its convective part, the heat flow can be expressed by relation (7) below:

$$\varphi_{gasFB-B}^{Conv} = h_{gasFB-B} \times A_{bed}^{l} \times \left(T_{gasFB} - T_{bed}\right) \quad (7)$$

where A_{bed}^{l} is the upper surface of the bed (Equation (7)) and a function of the geometric parameters of the kiln, T_{gasFB} the freeboard gas temperature (K), T_{bed} the bed temperature (K), and $h_{gasFB-B}$ the gas-solid convective exchange coefficient (W/m^2/K), whose value can be determined by correlations. Several correlations can be found in the literature to estimate $h_{gasFB-B}$. Babler et al. [84], Fan et al. [88], Liu et al. [90] and Mujumdar and Ranade [28] all proposed the following correlation (Equation (8)):

$$h_{gasFB-B} = 0.46 \times \frac{\lambda_g}{D_h} \times Re_D^{0.535} \times Re_\omega^{0.104} \times \eta^{-0.341} \quad (8)$$

The hydraulic diameter of the kiln D_h, Reynolds number (axial and angular) Re_D and Re_ω, and volume filling rate of the kiln η are derived from the equations given in [28, 81]. Agrawal and Ghoshdastidar [79] offered correlation (9) below to estimate the gas-solid heat exchange coefficient:

$$Nu_{Dh} = \frac{h_{gasFB-B} \times D_h}{\lambda_g} = \frac{(\xi_a/8) \times (Re_{Dh} - 1000) \times Pr}{1 + 12.7 \times (\xi_a/8)^{1/2} \times \left(Pr^{2/3} - 1\right)} \quad (9)$$

This correlation has been validated for Pr numbers between 0.5 and 2,000, and for Re_{Dh} numbers between 3,000 and 5×10^6; these values can be used for turbulent flow in a smooth pipe. ξ_a is Darcy's friction factor ($\xi_a = [0.79 \times ln(Re_{Dh}) - 1.64]^{-2}$), Nu_{Dh} and Re_{Dh} respectively the Nusselt number and Reynolds number, taken as a function of the hydraulic diameter D_h for the gas region. In their modeling studies of the calcination

of $CaCO_3$ in a rotary kiln, Küssel et al. [91] proposed a correlation similar to that of Agrawal and Ghoshdastidar [79], as given by relation (10) below:

$$Nu_{Dh} = \frac{(\xi_a/8) \times (Re_{Dh} - 1000) \times Pr}{1 + 12.7 \times (\xi_a/8)^{1/2} \times \left(Pr^{2/3}\right)} \times \left[1 + \left(\frac{D_h}{L_{kiln}}\right)^{\frac{2}{3}}\right] \quad (10)$$

with $\xi_a = [1.82 \times log(Re_{Dh}) - 1.64]^{-2}$, $2{,}300 < Re_{Dh} < 10^6$, and $D_h/L_{kiln} < 1$. Gunnarsson et al. [92], Huchet et al. [86] and Piton et al. [87] all used correlation (11) below, as established by Gorog et al. [93].

$$h_{gasFB-B} = 0.4 \times \left(\frac{3600 \times q_m^{gas}}{A_{gas}}\right)^{0.62} \quad (11)$$

where q_m^{gas} represents the mass flow rate of hot gases in the kiln (kg/s), and A_{gas} the cross-section of the gas phase in the rotary kiln (m^2). Studies conducted by Gorog et al.[93] evaluated the gas-solid exchange coefficient $h_{gasFB-B}$ at between 50 and 100 W/m^2/K, while Wes et al. [85] measured $h_{gasFB-B}$ values between 60 and 100 W/m^2/K. According to Wes et al. [85], these latter values can be found by the relation (12) below:

$$h_{gasFB-B} = 15 \times h_{gasFB-W} \quad (12)$$

where $h_{gasFB-W}$ is the coefficient of exchange by convection between the freeboard gas and the wall (W/m^2/K).

3.1.2.2. Gas-wall transfer

Several correlations in the literature allow assessing the gas-wall exchange coefficient, among which those of Tscheng and Watkinson [75], as utilized by Babler et al. [84], Lebas [89], Liu et al. [90], Mujumdar and Ranade [28], Colin [38] and Fan et al. [88], where Pr is the Prandtl number of gas. An order of magnitude for Pr has been located around 0.713 (for dry air at 1250°K) [94]. Gunnarsson et al. [92] presented a correlation similar to those of Tscheng and Watkinson [75], with the only difference being an extra multiplication factor k_G/D_e. Hausen [92, 93] proposed two correlations, one for the laminar regime ($Re_D < 2300$) the other for the transitional regime ($2300 < Re_D < 8000$), as respectively listed in Table 2. A correlation in the laminar regime is obtained for aspect ratios (L_{kiln}/D_{kiln}) equal to 0.5, 0.1 and 0.01. The correlation proposed by Küssel et al. [91] lies close to that given by Hausen [92, 93]. Huchet et al. [86], Piton [97], Piton et al. [87] and Seghir-Ouali et al. [98] all proposed correlation (13) below:

$$Nu = \frac{h_{gasFB-W} \times D_h}{\lambda_{gas}} = 0.02 \times Re_D^{0.93} + 8.5 \times 10^{-6} \times Re_\omega^{1.45} \quad (13)$$

The above correlation has been validated for Re_ω numbers lying between 1.6×10^3 and 4.7×10^5, as well as for Re_D numbers between 0 and 3×10^4. Agrawal and Ghoshdastidar [79] assumed that the coefficient of heat transfer by convection between gas and wall ($h_{gasFB-W}$) is less than that of gas-solid; they offered the following correlation (14):

$$h_{gasFB-W} = \frac{\lambda_{gas}}{D_h} \times \left(\frac{(\xi_a/8) \times (Re_{Dh} - 1000) \times Pr}{1 + 12.7 \times (\xi_a/8)^{1/2} \times \left(Pr^{2/3} - 1\right)}\right) \quad (14)$$

Riffaud and Koehret [99] proposed the following correlation (15) to estimate the convection exchange coefficient between gas and wall.

$$h_{gasFB-W} = 0.0981 \times \left(q_m^{gas}\right)^{0.67} \quad (15)$$

where q_m^{gas} is the mass flow of gases (in kg/s).

3.1.2.3. Exterior wall-ambient air transfer

The exterior wall-ambient air transfer is considered to be an energy loss (Figure 5); its intensity depends on the prevailing outdoor temperature conditions. Let's characterize its value by the relation (16):

$$\varphi_{wall-air}^{Conv} = h_{ext} \times A_{wall}^{ext} \times (T_{wall} - T_\infty) \quad (16)$$

with:

$$A_{wall}^{ext} = 2 \times \pi \times (R_{wall}^{ext})^2 \quad (17)$$

where T_{wall} is the temperature of the outer kiln wall (°K), T_∞ the ambient temperature (°K), h_{ext} the exterior wall-ambient air exchange coefficient, R_{wall}^{ext} the outside radius of the kiln (m), and A_{wall}^{ext} the outer surface of the kiln (m^2). Lebas [89] proposed two correlations for natural and forced convection; these correlations gave rise to the h_{ext} values of 0.26 W.m^{-2}.K^{-1} and 3-40 W.m^{-2}.K^{-1}, respectively for natural convection (with an exterior wall at 175°C, in 20°C ambient air) and for forced convection (with a wind speed of 4 to 100 km/h) [89]. Huchet et al. [86] and Piton et al. [87] also provided a correlation to estimate h_{ext}, based on Nusselt's number (see Table 3, where d_{kiln_ext} is the outer diameter of the rotary kiln (m), and λ_{air} the thermal conductivity of air (W/m/°K)). The above correlation has been validated for Re_ω numbers between 1.1×10^3 and 5.8×10^4, as well as for Re_∞ numbers between 0 and 3×10^4. Agrawal and Ghoshdastidar [79], and subsequently Gunnarsson et al. [92], proposed correlation (18) below:

$$h_{ext} = \frac{0.11 \times \lambda_{air}}{d_{kiln\_ext}} \times \left[\left(\frac{Re_\omega^2}{2} + Gr\right) \times Pr_{air}\right]^{0.35} \quad (18)$$

where Pr_{air} is the Prandtl number of the surrounding air. The Gr number of the above relationship is calculated according to the following relationship (19):

$$Gr = \frac{a_g \times \beta_{exp} \times \left(T_{kiln\_m} - T_\infty\right) \times d_{kiln\_ext}^3}{\nu_{air}} \quad (19)$$

where a_g is the gravitational acceleration (m/s^2), β_{exp} the coefficient of volumetric thermal expansion (1/K), T_{kiln_m} the average temperature of the outer wall (°K), and ν_{air} the kinematic viscosity of the ambient air (m^2/s). The literature also lists the numerical values of the coefficient h_{ext}. Marias et al. [10] provided a value of 20 W.m^{-2}.K^{-1} for the exchange coefficient h_{ext}, while E. Mastorakos et al. [76] produced a value of 30 W.m^{-2}.K^{-1}, which wound up being chosen when considering the fans used to cool the kiln tube (in the case of a cement plant).

3.1.2.4. Gas-to-free-falling grains

Li and Mason [100] numerically implemented a convective heat transfer coefficient for particle-laden flow in a dilute regime, such that:

$$\begin{cases} Nu_{cg} = 2 + \alpha_F^n \times 0.6 \times Re_p^{1/3} \times Pr^{1/3} & Re_p < 200 \\ Nu_{cg} = 2 + \alpha_F^n \times 0.5 \times Re_p^{1/2} + \alpha_F^n \times 0.02 \times Re_p^{0.8} \times Pr^{1/3} & 200 < Re_p < 1500 \\ Nu_{cg} = 2 + \alpha_F^n \times 4.5 \times 10^{-5} \times Re_p^{1.8} & Re_p > 1500 \end{cases} \quad (20)$$

with $Nu_{cg} = h_{cg} \times d_p/\lambda_S$, $Re_p = u_p \times d_p/\nu$ and α_F^n being the volume fraction of the gas phase; moreover, d_p is the particle diameter and λ_s the thermal conductivity of solids.

3.1.3. Heat transfer by radiation

Four possible exchanges can be encountered in the case of heat transfer by radiation in rotary kilns: gas-solid exchange, gas-wall exchange, wall-solid exchange, and exterior wall-ambient air exchange.

3.1.3.1. Gas-solid transfer

The thermal transfer between the gas phase and the solid phase in rotary kilns has been the subject of several research studies. Some authors have formulated it in the form of heat flux, while others in the form of an exchange coefficient or stretched exponential function of the gas and solid temperature [101]. Mujumdar and Ranade [28] proposed the relation in (21) to assess the radiative heat flow between the gas and the solid.

$$\varphi_{gasFB-B}^{Rad} = \sigma_B \times A_{bed}^l \times (\varepsilon_{bed} + 1) \times \left(\frac{\varepsilon_g \times T_{gasFB}^4 - \alpha_g \times T_{bed}^4}{2}\right) \quad (21)$$

where ε_{bed} is the emissivity of the bed, ε_g the freeboard gas emissivity, α_g the absorptivity of freeboard gas, and σ_B the Steffan-Boltzmann constant (5.67×10^{-8} W/m^2/K^4). This relationship is valid for both bed and gas emissivities greater than 0.8 [28]. Liu et al. [90] proposed a relation (Table 2) yielding a radiative exchange coefficient between the freeboard gas and the upper surface of the solid bed. Hanrot [73] published two relations (Table 2) in which the exchange surfaces were assumed to be isothermal. Specht [81] also proposed a relation (57), but in its infinitesimal form, in order to take into account temperature change along the kiln.
Fan et al. [88] derived the relation below (22) in order estimate $h_{gasFB-B}^{Rad}$.

$$h_{gasFB-B}^{Rad} = \varepsilon_{gas,bed} \times \sigma_B \times \left(T_{gasFB}^4 - T_{bed}^4\right)/\left(T_{gasFB} - T_{bed}\right) \quad (22)$$

where $\varepsilon_{gas,bed}$ is the effective emissivity of the gas to the bed of pellets. Lebas [89] also proposed this relation to estimate the radiant gas-solid heat flow.

3.1.3.2. Gas-wall transfer

The radiant gas-wall heat transfer in rotary kilns has interested many researchers, who have proceeded to model it as either a heat flux or a coefficient of exchange. Liu et al. [90] provided the following relation (23) to indicate the radiative exchange coefficient between the freeboard gas and the exposed wall:

$$h_{gasFB-W}^{Rad} = \varepsilon_{gas} \times F_{W-gas} \times \frac{E_{gas} - J_{wall}}{T_{gasFB} - T_{wall}} \quad (23)$$

where F_{W-gas} stands for the wall-freeboard gas form factor (-), E_{gas} the illumination (W/m^2), and J_{wall} the radiosity of the wall (W/m^2). Mujumdar and Ranade [28] established relationship (24) to estimate the radiative heat transfer between the gas and the exposed wall:

$$\varphi_{gasFB-W}^{Rad} = \sigma_B \times A_{wall}^{d} \times (\varepsilon_{wall} + 1) \times \left(\frac{\varepsilon_g \times T_{gasFB}^4 - \alpha_g \times T_{wall}^4}{2} \right) \quad (24)$$

where A_{wall}^{d} is the surface area of the exposed kiln wall (m^2), and ε_{wall} the emissivity of the interior kiln wall. Specht [81] proposed relation (25), in its infinitesimal form, to take into account temperature change along the kiln.

$$\frac{d\varphi_{gasFB-W}^{Rad}}{dA_{wall}^{d}} = \sigma_B \times \left(T_{gasFB}^4 - T_{wall}^4\right) \times \frac{1}{{}^1/_{\varepsilon_{gas}} + {}^1/_{\varepsilon_{wall}} - 1} \quad (25)$$

Lebas [89] proposed relation (26) below:

$$\varphi_{gasFB-W}^{Rad} = \sigma_B \times A_{wall}^{d} \times \psi_{gasFB-W}^{Rad} \times \left(T_{gasFB}^4 - T_{wall}^4\right) \quad (26)$$

Fan et al. [88] provided relation (27) to estimate $h_{gazFB-W}^{Ray}$.

$$h_{gasFB-W}^{Rad} = \varepsilon_{gas,kiln} \times \sigma_B \times \left(T_{gasFB}^4 - T_{kiln}^4\right) / \left(T_{gasFB} - T_{kiln}\right) \quad (27)$$

where $\varepsilon_{gas,kiln}$ is the effective emissivity of the gas to the kiln wall.

3.1.3.3. Wall-solid transfer

Several authors have carried out research on heat transfer by means of wall-solid radiation. As in the previous cases, the solid wall radiative transfer is modeled in the form of either a heat flux or an exchange coefficient. Mujumdar and Ranade [28] modeled the discovery wall-solid transfer by relation (28) below:

$$\varphi_{wall-B}^{Rad} = \sigma_B \times A_{bed}^{l} \times \varepsilon_{bed} \times \varepsilon_{wall} \times \Omega \times \left(T_{wall}^4 - T_{bed}^4\right) \quad (28)$$

where Ω is the radiation factor of the kiln, as given by relation (29):

$$\Omega = \frac{l_{bed}}{(2\pi - \varphi_{bed}) \times r_{kiln}} \quad (29)$$

where r_1 is the inner radius of the kiln (m), and l_{bed} the width of the solids bed (m).
Liu et al. [90] proposed relationship (30) to derive the radiative exchange coefficient h_{wall-B}^{Rad} between the wall and the upper surface of the solid bed:

$$h_{wall-B}^{Rad} = \left(1 - \varepsilon_{gas}\right) \times F_{B-W} \times \frac{J_{wall} - J_{bed}}{T_{wall} - T_{bed}} \quad (30)$$

where F_{B-W} is the bed-wall form factor (-), and J_{wall} the radiosity of the kiln (W/m^2). Specht [81] proposed relation (31), in its infinitesimal form, to take into account temperature change along the kiln.

$$\frac{d\varphi_{wall-B}^{Rad}}{dA_{wall}^{c}} = \sigma_B \times \left(T_{wall}^4 - T_{bed}^4\right) \times \frac{1}{{}^1/_{\varepsilon_{wall}} + {}^1/_{\varepsilon_{bed}} - 2 + {}^2/_{\left(2 - \varepsilon_{gas}\right)}} \quad (31)$$

3.1.3.4. Wall-to-external environment

The radiative transfer from the exterior wall to ambient air is of paramount importance for the estimation of heat losses from the rotary kiln towards the exterior. Specht [81] provided relation (32) to calculate the heat flow exchanged by radiation between the wall of the rotary kiln and ambient air:

$$d\varphi_{wall-air}^{Rad} = \sigma_B \times \varepsilon_{wall\_ext} \times \varphi_{kb} \times \left(T_{wall}^4 - T_{\infty}^4\right) \times dA_{wall}^{ext} \quad (32)$$

where ε_{wall_ext} denotes the emissivity of the sheet metal of the rotary kiln, φ_{kb} the view factor, A_{wall}^{ext} the surface area of the exterior wall of the kiln (i.e. the sheet) in m^2, and T_∞ the temperature of the external environment (K). Generally speaking, φ_{kb} can assume a value of unity or may be set at 0.5 [81].

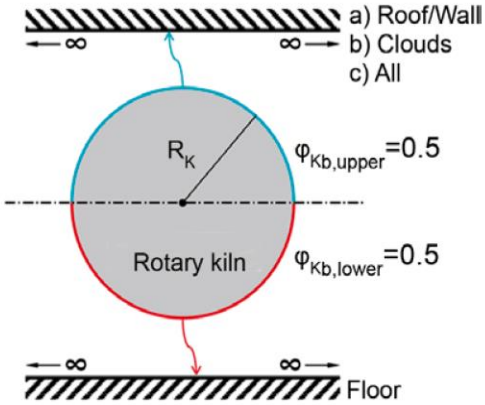

Figure 8: Heat dissipation by radiation from the outer shell surface to the environment [81]

According to Specht [81], the heat loss caused by radiation from a rotary kiln depends on its location, namely whether the lower half or upper half of the rotary kiln. Figure 8 shows that the lower half of the rotary kiln always radiates to the ground, which embodies the ambient temperature, while the upper half of the rotary kiln radiates to the hall walls (should the rotary kiln be installed in a hall), which also measure at approximately ambient temperature. The expression proposed by Nørskov [102] is given for $\varphi_{kb} = 1$. Since the kiln sheet is often made of highly oxidized steel, the value of ε_{wall_ext} lies very close to unity. Lebas [89] estimated this value at between 0.9 and 1. For Specht [81], in a dry, cloud-free atmosphere, ε_{wall_ext} equals about 0.81 and in a humid cloudy atmosphere $\varepsilon_{wall\_ext} = 0.53$. Fan et al. [88] and Liu et al. [90] both proposed the following relation to determine the radiative exchange coefficient $h_{wall-air}^{Rad}$ between the outer wall of the rotary kiln and the surrounding environment (Equation (33)):

$$h_{wall-air}^{Rad} = \sigma_B \times \varepsilon_{wall} \times \frac{T_{wall\_ext}^4 - T_\infty^4}{T_{wall\_ext} - T_\infty} \tag{33}$$

where T_{wall_ext} is the temperature of the outer wall (K).

3.1.4. Particle-to-particle heat transfer

Particle-to-particle heat transfer plays a key role in the exchange between a wall and a bed of solids and/or between a gas and a bed of solids. This transfer has also been the subject of several publications. Chang et al. [103] presented a computational study of heat transfer, with emphasis on the direct particle-to-particle heat transfer between different classes of particles in a dense gas-solid fluidized bed of binary particles using the computational fluid dynamics (CFD) method. The results of their study showed that the particle-particle heat exchange coefficient between different classes of particles increases with increasing particle size and gas surface velocity. Felinks et al. [104] undertook an experimental study of the heat transfer between these two particle species in a binary packed bed, in the context of heat recovery via a particulate redox material. Their resultant heat transfer coefficient values lie between 90 and 260 W/m2 K, as obtained after solving a polynomial equation (Equation (34)).

$$\alpha = C_0 + C_1\tau + C_2 t \tag{34}$$

where τ is the contact time (s), and t the average temperature (°C). Coefficients C_0, C_1 and C_2 are found to have the following values respectively: 2.157E+02, -7.533E+00, and 3.871E-01.

Chang et al. [105] developed a collisional particle-to-particle heat transfer model within the scope of the Eulerian-Eulerian approach. They also found that the particle-to-particle heat exchange coefficient between different classes of particles increases with increasing particle size and gas surface velocity. Gui et al. [106] focused on investigating the factors involved in particle-particle heat exchange, including rotational speed. These authors claimed to have achieved the maximum efficiency of particle-particle heat conduction. Saruwatari and Nakamura [19] also investigated the behavior of coarse grains and heat transfer in a rotary kiln; they went on to propose a coarse grain method for the so-called "Hertz-Mindlin contact", which is based on rolling friction and conductive heat transfer between particles.

3.2. Critical analysis

From a practical perspective, certain correlations within a convective regime between the gas and the wall (inner and outer) or the particles (bed, falling particles) lie outside their range of validity. Indeed, it has been remarked that various changes of geometry can occur in RK when developing gas phase flows. The example of a sudden enlargement from the duct burner to the RK diameter is responsible for an increase in the gas-wall heat transfer coefficient, observed to be six times higher than the fully developed duct flow. Specht [81] argued that secondary flows (Figure 9) can contribute to this increase. Similar aerodynamics phenomena of secondary flow occurrence have been observed in RK equipped with additional material inlets [128].

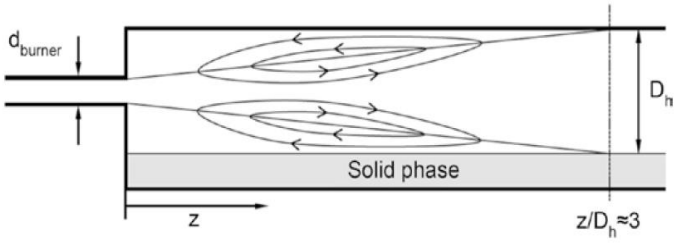

Figure 9: Kiln inlet gas flow caused by a burner [81]

A second aspect deserving of attention herein is the assessment of a solid/wall heat transfer coefficient. This issue remains highly debated and encountered with any kind of rotary kiln geometry. In the case of direct transmission, i.e. where the kiln is heated by means of gas produced by the burner, the direction of the solid/wall exchange can be reversed (i.e. from the solid to the wall), whenever the load progresses along the kiln [70, 74, 104, 105], while in the case of indirect transmission (heating by the walls, and possibly regeneration), the exchange is naturally always performed to benefit the load. Colin [38], Hanrot [73] and Lybaert [78] stated that a sound model would likely be one that takes into account all of the heat fluxes present. The model produced by Mujumdar and Ranade [28] only takes into account the transfer to the bed. The Ginsberg and Modigell model [65] takes into account two fluxes: the wall-solid contact resistance, and the resistance of penetration into the solid mass. The models by Babler et al. [84] and Liu et al. [90] are also based on two resistances in series: resistance caused by the film of gas surrounding the particle, and resistance caused by the bed material itself. Lybaert [78] listed the various possible flows: transfer into the solid, walls-solid contact resistance, and an inhomogeneous zone containing a solid fraction and a gas fraction.

Table 2: Heat transfer models

CONDUCTION								
Covered wall-to-Solid								
Equations	$h_{wall-B} = 11.6 \times \frac{\lambda_{bed}}{A^c_{wall}} \times \left(\frac{\omega \times r^2_{kiln} \times \delta_{bed}(z}{D_{bed}}$	$\frac{1}{h_{wall-B}} = \frac{1}{(h_{wall-B})_{wall}} + \frac{1}{(h_{wall-B})_B}$	$h_{wall-B} = 2 \times \sqrt{\frac{\lambda_{bed} \times (\rho \times Cp)}{\pi \times t_c}}$	$\frac{1}{h_{wall-B}} = \frac{\chi_{ks} \times d_p}{\lambda_{gas}} + \frac{1}{2} \times \left(\frac{2 \times \lambda_{bed} \times (\overline{\rho \times C_p}) \times n_{kiln}}{(\delta_{bed}/2)}\right.$	$ln\frac{T_{wall} - T_{wallc}(}{T_{wall} - T_{lit}} = -\frac{h_{wall-B} \times A^c_w}{Cp_{bed} \times m_b} \times t$	$h_{wall-B} = 11.6 \times \frac{\lambda_{bed}}{2 \times \delta_{bed} \times r_{kiln}} \times \left(\frac{2 \times \omega \times r^2_{kiln} \times \delta_{bed}(z}{D_{bed}}\right.$	$h_{wall-B} = \sqrt{\frac{\lambda_{bed} \times \rho_{bed} \times Cp}{\pi \times t_c}} + \frac{2 \times \lambda_{gas}}{d_p} \times \left\{\left[\frac{\delta_{gf} + \gamma_f}{d_p}\right] \times ln\left[\frac{d_p}{\delta_{gf} + \gamma_f} + 1\right] - 1\right\}$	$h_{wall-B} = \left\{\chi_{exp} \times \frac{d_p}{\lambda_{gas}} + \left[2 \times \sqrt{\frac{\lambda_{bed} \times \rho_{bed} \times Cp_{bed}}{\pi \times t_c}}\right]^{-}\right.$
Original Authors	Tscheng and Watkinson [75]	Schlünder and Mollekopf [109]	Wes et al. [85]	Li et al.[83]	Wes et al. [85]	Tscheng and Watkinson [75]	Fan et al. [88]	Tscheng and Watkinson [75]
Users (Authors)	Tscheng and Watkinson [75], Csernyei and Straatman [74], and Mujumdar and Ranade [28], Mungyeko Bisulandu and Marias [110]	Schlünder and Mollekopf [109], Ginsberg and Modigell [65]	Wes et al. [85], Shi et al. [80], Lehmberg et al. [111]	Li et al.[83], Babler et al. [84]	Wes et al. [85]	Tscheng and Watkinson [75]	Fan et al. [88]	Liu et al. [90]
CONVECTION								
Gas-to-Solid								
Equations	$h_{gasFB-B} = 0.46 \times \frac{\lambda_g}{D_h} \times Re_D^{0.535} \times Re_\omega^{0.104} \times \eta^{-0.341}$			$Nu_{Dh} = \frac{(\xi_a/8) \times (Re_{Dh} - 1000) \times Pr}{1 + 12.7 \times (\xi_a/8)^{1/2} \times \left(Pr^{2/3} - 1\right)}$				$h_{gasFB-B} = 15 \times h_{gasFB-W}$

		$Nu_{Dh} = \frac{(\xi_a/8) \times (Re_{Dh} - 1000) \times Pr}{1 + 12.7 \times (\xi_a/8)^{1/2} \times \left(Pr^{2/3}\right)} \times \left[1 + \left(\frac{D_h}{L_{kiln}}\right)^{\frac{2}{3}}\right]$		$h_{gasFB-B} = 0.4 \times \left(\frac{3600 \times q_m^{gas}}{A_{gas}}\right)^{0.62}$	
Original Authors	Tscheng and Watkinson [75]	Küssel et al. [91]	Gnielinski [112]	Gorog et al.[93].	Wes et al.[85]	
Users (Authors)	Babler et al. [84] , Fan et al. [88], Liu et al. [90], and Mujumdar and Ranade [28], Granados et al. [31], Machalek and Powell [113], Urbano et al. [114]	Küssel et al. [91]	Gnielinski [112], Agrawal and Ghoshdastidar [79]	Gorog et al.[93], Gunnarsson et al. [92]	Wes et al.[85]	
Gas-to-Wall						
Equations	$h_{gasFB-W} = 1.54 \times \frac{k_G}{D_e} \times Re_D^{0.575} \times Re_\omega^{-0.292}$ $h_{gasFB-W} = 0.036 \times Re_D^{0.8} \times Pr^{0.33} \times \left(\frac{D_{kiln}}{L_{kiln}}\right)^{0.055}$	1) Laminar case $Nu = 3.66 + \frac{0.0668 \times Re_D \times Pr \times (D_{kiln}/L_k}{1 + 0.04 \times [Re_D \times Pr \times (D_{kiln}/L_{kil}}$ 2) Turbulent case $Nu = 0.0235 \times (Re_D^{0.66} - 125) \times \left[1 + \left(\frac{D_{kiln}}{L_{kiln}}\right)^{0.66}\right]$	$Nu = 0.0214 \times (Re_D^{0.8} - 100) \times Pr^{0.4} \times \left[1 + \left(\frac{D_{kiln}}{L_{kiln}}\right)^{0.66}\right]$	$Nu = \frac{h_{gasFB-W} \times D_h}{\lambda_{gas}} = 0.02 \times Re_D^{0.93} + 8.5 \times 10^{-6} \times Re_\omega^{1.45}$	$h_{gasFB-W} = \frac{\lambda_{gas}}{D_h} \times \left(\frac{(\xi_a/8) \times (Re_{Dh} - 1000) \times Pr}{1 + 12.7 \times (\xi_a/8)^{1/2} \times \left(Pr^{2/3} - 1\right)}\right)$	$h_{gasFB-W} = 0.0981 \times \left(q_m^{gas}\right)^{0.67}$
Original Authors	Tscheng and Watkinson [75]	Hausen [95,96]	Küssel et al. [91]	Seghir-Ouali et al. [98]	Gnielinski [112]	Riffaud and Koehret [99]
Users (Authors)	Tscheng and Watkinson [75], Babler et al.[84], Lebas [89], Liu et al.[90], Mujumdar and Ranade [28], Colin	Hausen [95,96], Seghir-Ouali et al. [98]	Küssel et al. [91]	Seghir-Ouali et al. [98]	Gnielinski [112], Agrawal and Ghoshdastidar [79]	Riffaud and Koehret [99]

	[38], and Fan et al.[88], Urbano et al. [114] Machalek and Powell [113], Gunnarsson et al. [92]					
Exterior wall-to-Ambient air						
Equations	$Nu = 0.6 + \frac{0.387 \times Ra^{1/6}}{\left[1 + \left(\frac{0.559}{Pr}\right)^{9/16}\right]^{8/27}}$ $Nu = 0.3 + \frac{0.62 \times Re^{1/2} \times Pr^{1/3}}{\left[1 + \left(\frac{0.4}{Pr}\right)^{2/3}\right]^{1/4}} \times \left[1 + \left(\frac{Re}{282000}\right)^{a}\right]^{b}$	$Nu = 0.11 \times \left(\frac{Re_\omega^2}{2} + Gr\right) \times Pr^{0.35}$	$Nu = \frac{h_{ext} \times d_{kiln\_ext}}{\lambda_{air}} = 0.135 \times \left(\frac{Re_\omega^2}{2} + Re_\infty^2 + Gr\right)^{1/3}$	$h_{ext} = \frac{0.11 \times \lambda_{air}}{d_{kiln\_ext}} \times \left[\left(\frac{Re_\omega^2}{2} + Gr\right) \times Pr_{air}\right]^{0.35}$	$h_{ext} = \frac{0.11 \times \lambda_{air}}{d_{kiln\_ext}} \times \left[\left(\frac{0.5 \times Re_\omega^2}{2} + Gr\right) \times Pr_{air}\right]^{0.35}$
Original Authors	Özışık [115]	Sucec [116]	Kays and Bjorklund [117]	Barr et al.[77]	Barr et al.[107]	
Users (Authors)	Özışık [115], Lebas [89]	Sucec [116], Hanrot [73]	Kays and Bjorklund [117], Labraga and Berkah [118]	Agrawal and Ghoshdastidar [79], and Gunnarsson et al. [92]	Fan et al. [88]	
Gas-to-Free-falling grains						
Equations	$Re_p < 200$ $Nu_{cg} = 2 + \alpha_F^n \times 0.6 \times Re_p^{1/3} \times Pr^{1/3}$		$200 < Re_p < 1500$ $Nu_{cg} = 2 + \alpha_F^n \times 0.5 \times Re_p^{1/2} + \alpha_F^n \times 0.02 \times Re_p^{0.8} \times Pr^{1/3}$		$Re_p > 1500$ $Nu_{cg} = 2 + \alpha_F^n \times 4.5 \times 10^{-5} \times Re_p^{1.8}$	
Original Authors	Li and Mason [100]		Li and Mason [100]		Li and Mason [100]	
Users (Authors)	Li and Mason [100]		Li and Mason [100]		Li and Mason [100]	
RADIATION						
Gas-to-Solid						

Equations	$\varphi_{gasFB-B}^{Rad} = \sigma_B \times A_{bed}^{l} \times (\varepsilon_{bed} + 1) \times \left(\frac{\varepsilon_g \times T_{gasFB}^4 - \alpha_g \times T_{bed}^4}{2}\right)$	$\varphi_{gasFB-B}^{Rad} = \sigma_B \times \left(T_{gasFB}^4 - T_{bed}^4\right) \times \frac{1}{1/\varepsilon_{gas} + 1/\varepsilon_{bed} -}$ $\varphi_{gasFB-B}^{Rad} = \left(\frac{\varepsilon_{bed} + 1}{2}\right) \times \sigma_B \times \left(\varepsilon_{gas} \times T_{gasFB}^4 - \alpha_{gas} \times T_{bed}^4\right)$	$h_{gasFB-B}^{Rad} = \varepsilon_{gas,bed} \times \sigma_B \times \left(T_{gasFB}^4 - T_{bed}^4\right)/\left(T_{gasFB} - T\right.$	$\varphi_{gasFB-B}^{Rad} = \sigma_B \times A_{bed}^{l} \times \psi_{gasFB-B}^{Rad} \times \left(T_{gasFB}^4 - T_{bed}^4\right)$	$h_{gasFB-B}^{Rad} = \varepsilon_{gas} \times F_{B-gas} \times \frac{E_{gas} - J_{bed}}{T_{gasFB} - T_{bed}}$
Original Authors	Hottel and Sarofim [119]	Barr [120]	Manitius et al.[121]	Manitius et al.[121]	Gorog et al.[93]
Users (Authors)	Hottel and Sarofim [119], Mujumdar and Ranade [28]	Barr [120], Hanrot [73]	Manitius et al.[121], Fan et al. [88]	Manitius et al.[121], Lebas [89]	Gorog et al.[93], Liu et al. [90]
Gas-to-Wall					
Equations	$h_{gasFB-W}^{Rad} = \varepsilon_{gas} \times F_{W-gas} \times \frac{E_{gas} - J_{wall}}{T_{gasFB} - T_{wall}}$	$\varphi_{gasFB-W}^{Rad} = \sigma_B \times A_{wall}^{d} \times \psi_{gasFB-W}^{Rad} \times \left(T_{gasFB}^4 - T_{wall}^4\right)$	$h_{gasFB-W}^{Rad} = \varepsilon_{gas,wall} \times \sigma_B \times \left(T_{gasFB}^4 - T_{kiln}^4\right)/\left(T_{gasFB} - T_{kiln}\right)$	$\varphi_{gasFB-W}^{Rad} = \sigma_B \times A_{wall}^{d} \times (\varepsilon_{wall} + 1) \times \left(\frac{\varepsilon_g \times T_{gasFB}^4 - \alpha_g \times T_{wall}^4}{2}\right)$
Original Authors	Gorog et al.[93]	Manitius et al.[121]	Manitius et al.[121]	Hottel and Sarofim [119]
Users (Authors)	Gorog et al.[93], Liu et al. [90]	Manitius et al.[121], Lebas [89]	Manitius et al.[121], Fan et al. [88]	Hottel and Sarofim [119], Mujumdar and Ranade [28]
Wall-to-Solid				
Equations	$\varphi_{wall-B}^{Rad} = \sigma_B \times A_{bed}^{l} \times \varepsilon_{bed} \times \varepsilon_{wall} \times \Omega \times (T_{wall}^4 - T_{bed}^4)$	$\varphi_{wall-B}^{Rad} = \sigma_B \times A_{bed}^{l} \times \psi_{wall-B}^{Rad} \times (T_{wall}^4 - T_{bed}^4)$	$h_{wall-B}^{Rad} = \varepsilon_{wallB,g} \times \sigma_B \times (T_{wall}^4 - T_{bed}^4)/(T_{wall} - T_{bed})$	$h_{wall-B}^{Rad} = \left(1 - \varepsilon_{gas}\right) \times F_{B-W} \times \frac{J_{wall} - J_{bed}}{T_{wall} - T_{bed}}$
Original Authors	Mujumdar and Ranade [28]	Manitius et al.[121]	Manitius et al.[121]	Gorog et al.[93]
Users (Authors)	Mujumdar and Ranade [28]	Manitius et al.[121], Lebas [89]	Manitius et al.[121], Fan et al. [88]	Liu et al.[17]
Exterior wall-to-Ambient air				
Equations	$\varphi_{wall-air}^{Rad} = \sigma_B \times \varepsilon_{wall\_ext} \times A_{wall}^{ext} \times (T_{wall}^4 - T_{\infty}^4)$	$\varphi_{wall-air}^{Rad} = \alpha_{wall} \times \left(T_{wall\_ext} - T_{\infty}\right) + T_{wall\_ext} - T_{\infty} + \sigma_B \times \varepsilon_{wall} \times T_{wall\_ext}^4 - T_{\infty}^4$	$h_{wall-air}^{Rad} = \sigma_B \times \varepsilon_{wall} \times \frac{T_{wall\_ext}^4 - T_{\infty}^4}{T_{wall\_ext} - T_{\infty}}$	

Original Authors	Nørskov [102]	Mintus et al.[55]	Gorog et al.[93]	
Users (Authors)	Nørskov [102]	Mintus et al.[55]	Ginsberg and Modigell [65], Fan et al. [88], Liu et al. [90]	

4. Thermochemical conversion in rotary kilns: Applications

Since the rotary kiln is an equipment used in several solid treatment processes, its modeling depends on the process used. Three specific case studies will now be presented: the first is an application in cement manufacturing; the second pertains to waste and biomass treatment in kilns; and the last one relates to other applications. Kinetic models of rotary kilns are more specifically dedicated to the thermochemical conversion process, either cement meal, waste and biomass, or even other materials. The literature is extremely limited on the thermochemical conversion in cement kilns. Babler et al. [84] developed an unsteady 1D pyrolysis model of biomass in the rotary kiln in order to optimize bio-char production; this model is based on the mass and energy conservation equations. The model also includes independent sub-models dedicated to the pyrolysis reaction, heat transfer and granular flow in the rotary kiln. The authors noticed that increased rotational speed of the kiln causes a decrease in residence time; in contrast, it also allows for a good granular mixture in the solids bed, which serves to improve heat transfer and manifests itself by a rapid increase in bed temperature. Ariyaratne et al. [122] argued that biomass fuels are not only greenhouse gas-neutral but also have the potential to mitigate such impacts since these fuels will otherwise produce methane and other decomposition products during decay. These gases greatly exceed the potency of CO_2 as greenhouse gases. Mungyeko Bisulandu and Marias [110] developed a one-dimensional model of the thermochemical conversion of biomass in cement rotary kilns. They asserted that the drying and pyrolysis steps were performed quickly, given the temperature level of the cement kilns, and moreover that the chemical reactions were of the first order. In their work on the CFD modeling of meat and bone meal combustion in a cement rotary kiln, Ariyaratne et al. [122] investigated the effects of fuel supply, as well as both the effects and impacts of fuel particle size on combustion. Their results showed that devolatilization occurs much faster in the case of small particles, hence their conclusion: "For a given fuel, the higher the mass-weighted average particle diameter, the lower the coal depletion". They also posited that the negative effect of a large weighted average particle size on coal depletion is greater for fixed high carbon fuels. Nielsen [69] studied the devolatilization and combustion of tires and pinewood in a pilot-scale rotary kiln, under conditions similar to those at the input end of the meal into rotary kilns. Marias et al. [10] presented a mathematical model, with three sub-models (bed model, furnace model, gas model) for the pyrolysis of aluminum scrap, in the aim of predicting the physicochemical processes when this waste is introduced into the rotary kiln. Their model is mainly based on a description and coupling of the first two models.

4.1. The cement manufacturing case

Many works in the literature pertain to the modeling of rotary kilns for cement production. Cement rotary kilns can be modeled in terms of various aspects, including those relative to load transport, cement chemistry, chemistry and waste combustion physics (in the case of waste substitution), thermal transfers in the bed, in the gases and in the walls of the kiln, etc. Aside from the thermal and load transport models, the literature contains several works modeling cement rotary kilns with the following set-up.

4.1.1. Three sub-models (solid phase, gas phase, kiln shell)

The modeling of rotary kilns in three sub-models has become increasingly used in recent times. E. Mastorakos et al. [76] presented a rotary kiln model that takes into account thermochemical phenomena in: the gas phase (including a study of gas radiation), the solid phase (consisting only of cement meal), and the kiln walls. The last model has been obtained after coupling the gas-solid-wall parts; this model has revealed that radiation is the dominant mode of gas-wall heat transfer in the oven, as compared to convection. Spang [123] proposed a dynamic 1D model of the cement kiln, aimed at understanding how the process works, in order to come up with a way to improve it. This model includes the solid phase, which is essentially characterized by the thermochemistry of clinkering reactions, and the gas phase, characterizing the temperature of the flame produced by coal/fuel oil combustion. According to this model, the temperatures of solids and gases solely depend on the axial position in the kiln, while the wall temperature only depends on time. As for the dynamic behavior, Spang [123] noted that the exothermic reactions of the burning flame and those of C_2S in the solid cause a retroactive situation that induces high temperatures in both the clinkering (solid phase) and combustion (gas phase) zones of the kiln. Similar behavior has been reported when recycled pavement materials are injected into an asphalt

mixing plant undergoing a temperature rise [86]. Wang et al. [124] proposed a model for burning coal in the cement kiln; they considered several models during their studies: the bed model (in consideration of the chemical reactions of clinkerization), the gas-solid flow model (coal combustion), and the thermal model in the clinkerization zone. The main objective of their model was to analyze the physicochemical processes of clinker formation, using a heat flux function, and couple the various models in order to predict the temperature and composition profiles of gaseous species along the rotary kiln. Mungyeko Bisulandu and Marias [110] also provided a model subdivided into three sub-models: solid phase, gas phase, and kiln shell. Modeling in three sub-models is employed as well in other rotary kiln applications.

4.1.2. Five model reactions of clinkering

The mechanism for transforming meal into clinker is most often described in the literature by the following five reactions (Equation (35)):

$$\begin{gathered} CaCO_3 \rightarrow CaO + CO_2 \\ 2CaO + SiO_2 \rightarrow (CaO)_2 \times (SiO_2)\ or\ C_2S \\ C_2S + CaO \rightarrow C_2S \times (CaO)\ or\ C_3S \\ 3CaO + Al_2O_3 \rightarrow (CaO)_3 \times (Al_2O_3)\ or\ C_3A \\ 4CaO + Al_2O_3 + Fe_2O_4 \rightarrow (CaO)_4 \times (Al_2O_3) \times (Fe_2O_4)\ or\ C_4AF \end{gathered} \tag{35}$$

Mujumdar and Ranade [28] and Mungyeko Bisulandu and Marias [110] developed a bed model that takes into account just five reactions for clinker formation. Hiromi Ariyaratne et al. [125] presented a mathematical model that also takes into account five major chemical reactions of the solid inside the rotary kiln, e.g. calcination, endothermic fusion and exothermic clinkering. Bhad et al. [126], Darabi [127], E. Mastorakos et al. [76] and Spang [123] also modeled clinker formation reactions using the five reactions listed above.

4.1.3. Solid fusion and the additional layer

It is important to consider the melting of part of solids in the bed plus the formation of an additional layer in the walls of the cement rotary kiln. Mujumdar and Ranade [28] and E. Mastorakos et al. [76] took into account the formation of the additional layer of clinker in the interior walls of the furnace, as well as the formation of the liquid phase in the solids bed; such is not the case in the works of Spang [123], Mungyeko Bisulandu and Marias [110], and Darabi [127]. Mujumdar and Ranade [28] considered that the additional clinker layer only forms in the clinkering zone, subsequent to material fusion (mainly due to C_4AF formation). E. Mastorakos et al. [76] considered that the additional layer of clinker in the kiln walls is uniform along the kiln. Many models in the literature actually neglect this feature, in an effort to reduce model complexity.

4.1.4. Partial substitution of waste and biomass

Very few works in the literature focus on the substitution of waste and biomass in cement rotary kilns. Kaantee et al. [128] modeled a rotary kiln for cement production using alternative fuels. The primary objective of their study was to optimize process control when alternative fuels are introduced, in order to maintain the quality of the clinker. Nielsen [69] studied the devolatilization and combustion of tires and pinewood in a pilot scale rotary kiln, under conditions similar to those at the inlet end of meal (raw materials) in rotary kilns. Mungyeko Bisulandu and Marias [110] developed a stationary 1D model for the thermochemical conversion of biomass in a cement rotary kiln in order to supply the energy needs for the production of cement clinker. This model is based on the mass and energy conservation equations. Table 3 below summarizes all of the foregoing discussion.

Table 3: Recap of the models studied herein

Authors	3 sub-models	5 model reactions	Solid fusion	Waste substitution
Darabi [127]	**Yes**	**Yes**	**No**	**Yes**
E. Mastorakos et al. [76]	**Yes**	**Yes**	**Yes**	**No**
Spang [123]	**Yes**	**Yes**	**No**	**No**
Mujumdar and Ranade [28]	**No**	**Yes**	**Yes**	**No**

Kaantee et al. [128]	**No**	**No**	**No**	**Yes**
Nielsen [69]	**No**	**No**	**Yes**	**Yes**
Mungyeko Bisulandu and Marias [110]	**Yes**	**Yes**	**No**	**Yes**
Wang et al. [124]	**No**	**No**	**No**	**Yes**
Hiromi Ariyaratne et al. [125]	**-**	**Yes**	**-**	**Yes**
Bhad et al. [126]	**-**	**Yes**	**-**	**-**

4.2. Waste and biomass treatment cases

Different types of waste and biomass treatment models apply to rotary kilns. Marias et al. [10] presented a mathematical model, composed of three sub-models (bed model, kiln model, gas model), for the pyrolysis of aluminum waste in order to predict the physicochemical processes once the waste has been introduced into the rotary kiln. Colin et al. [129] offered a model for roasting wood chips in the rotary kiln. These authors used Saeman's model [36] to study the flow of load into the kiln to predict the residence time and loading profile of the bed. Babler et al. [84] developed a stationary 1D model for the pyrolysis of biomass in a rotary kiln to optimize the production of bio-char; their model is based on the mass and energy conservation equations, in addition to including independent sub-models dedicated to the pyrolysis reaction, heat transfer and granular flow taking place inside the kiln. Babler et al. [84] noted that increasing the rotational speed of the kiln leads to a reduction in residence time, while allowing for an effective granular mixture in the solids bed, which according to them improves heat transfer, as manifested by a rapid increase in bed temperature. Babler et al. [84] and Colin et al. [129] used Saeman's model [36] to describe granular flow in a rotary kiln. Babler et al. [84] furthermore claimed that heat transfer and granular flow are both controlled by the kiln's rotational speed. Marias [130] forwarded the assumption that the bed receives both the specific heat flow from the gas phase and a specific heat flow from the kiln walls. Huchet et al. [86] and Le Guen et al. [131] proposed adding an equation once a new phase (heat waste and/or reclaimed asphalt products) has been added to the system, under the assumption that the heat exchange coefficients had been previously determined [132].

4.3. Other models

Several technologies exist for the heat treatment of a wide variety of materials and products from rotary kiln; these can be divided into three categories:

- The direct heated rotary kiln with lifter flights is characterized by baffles of a rectangular L-shape (but other shapes can also be used) to promote mixing in the transverse section of the kiln. This set-up ensures a homogeneous heat transfer and high rate of conversion of chemical reaction or drying kinetics. Its advantage lies in the design of shorter facilities [133], while its disadvantage is the presence of a thermal runaway, which can provoke ignition or deterioration of the products [86]. Another disadvantage is an entrainment of fines into the gas flow and, in some cases, the additional production of fines due to higher energy collisions.
- The direct heated rotary kiln is the most popular technology and has been designed for clinker production and coal treatment. These facilities feature a longer tube, which serves to raise the mass flow rate of production.
- The indirect heated rotary kiln is less widespread; it can operate either with flight or without flight and has recently been more extensively studied within the scope of waste-to-energy gasifiers (e.g. pyrolysis of biomass). Its advantage lies in a better control over the heat treatment to help guarantee process safety.

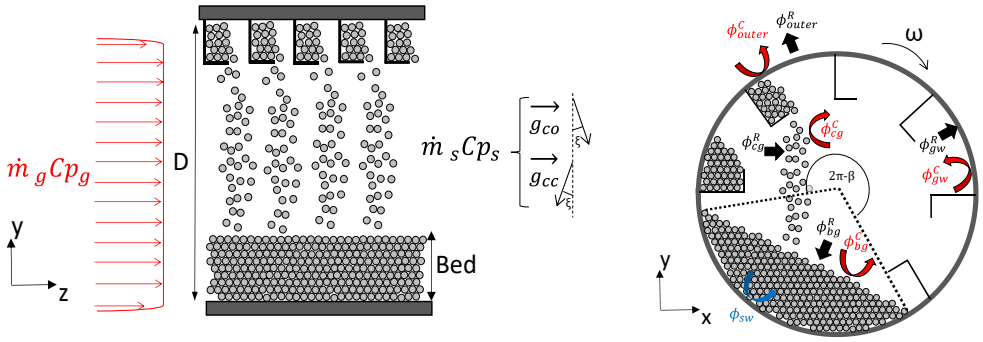

Figure 10: Granular motion for a rotary kiln composed of L-lifters (extracted from [131])

In the case of a flight rotary kiln, in addition to the parameters calculated for a smooth rotary kiln, it is important to quantify the number of materials loaded in each flight so as to establish a suitable discharge law to quantify the transverse surface of the granular cascade, according to:

$$f_T = f_F + f_C + f_B \tag{36}$$

with f_F being the filling degree in the flight, f_c the filling degree in the granular cascade and f_B the filling degree of the bed.

The filling degree in the flight f_F and the filling degree of the curtain materials f_c are both calculated at any angle of rotation, δ. Sunkara et al. [134] distinguished three possibilities of flight filling (complete, partial or limited filling) to evaluate the flight hold-up that depends on geometric parameters as well as the angular positioning of the flight. f_c can therefore be computed from the following equation:

$$f_{C,i}(\delta) = \sqrt{2 \times Fr \times \frac{h_F(\delta)}{d_{kiln}/2}} \times \left(\frac{f_{F,i}(\delta)}{d\delta}\right) \tag{37}$$

with h_F being the height of the fall (in m).

The relevance of such a granular transport model has been demonstrated in a direct heated flight rotary kiln used for pavement production [87].

5. Current status, challenges and the future direction of technology

Rotary kilns are used in many industrial applications, mainly in the cement industry. The scarcity and depletion of fossil fuels (which has promoted the reliance on alternative energies), as well as the management of gaseous emissions and fine particles in the atmosphere constitute real challenges facing rotary kilns, particularly those involved with cement production. The emissions issue remains a major challenge, encompassing both CO_2 capture and sequestration, NOx and SOx trapping, and solid pollutants. Other challenges faced by rotary kilns include: energy optimization (recovery, storage and recovery of waste heat from the kiln, optimization of process control laws, etc.), the use of completely carbon-free energy (e.g. concentrated solar energy), and an automated and optimal control and supervision of the rotary kiln that take into account all the process operating parameters.

5.1. Management of gaseous emissions and fine particles

In recent decades, environmental protection has become such an important global issue that several current research works are focused on improving existing methods to make industry less polluting [135]. Pollutant emissions in the cement plant are linked to parameters that need to be addressed: combustion of fossil fuels (adjustment of various geometric parameters of the burner [136], production of fine particles, etc.), combustion of alternative fuels (rapid pyrolysis favoring a high content of volatiles, production of fine particles, etc.), clinkering reactions (alkali metal sulfates in raw meal, etc.), and reduction reactions and gaseous reactions in the homogeneous phase. Gases such as CO_2, SOx, NOx, H_2S and VOCs from various thermochemical processes are emitted into the atmosphere and cause damage (global warming, respiratory disorders, etc.) [137]. The polluting nature of the cement industry is no longer in doubt. Pollutant emissions in cement works stem mainly from the combustion of fossil fuels and the decarbonation of limestone [11]. Emissions from electricity consumption are often much lower. Several gaseous compounds are emitted in the smoke or gas exiting the kiln, namely: CO_2, CO,

NOx, SOx, and O_2. CO_2 is the primary gas produced in the cement plant; it stems from the decarbonation reaction of $CaCO_3$; when considering its share of CO_2 production, this reaction accounts for more than an estimated 60% of the overall CO_2 emissions from the process [12, 133]. Thus, the production of 1 kg of clinker emits 0.471 kg eq CO_2 by the decarbonation of limestone (i.e. 128 g eq °C) and 0.314 kg eq CO_2 by the combustion of fossil resources (i.e. 86 g eq °C). This amounts to a total of 0.785 kg eq CO_2 (or 214 g eq °C) [11]. According to the International Energy Agency (IEA), cement plants worldwide are expected to generate 2.34 billion tons of CO_2 in 2050 [133-137]. In an effort to solve this problem, several researchers have conducted detailed investigations. According to Mutlu et al. [142], biomass is preferred to fossil fuels because it generates less CO2 emissions. Mishra et al. [137] suggested the use of compounds with characteristics similar to clinker, in order to reduce energy consumption and therefore reduce emissions due to the formation of clinker. For Hills et al. [138], significantly reducing CO_2 emissions in cement kilns could prove to be difficult or costly without carbon capture and storage. According to these authors, it is difficult to apply precombustion capture to industrial processes due to the nature of the emissions, with such a technique often being more expensive and energy intensive. Figure 11 shows the CO_2 emissions caused by calcining limestone, in different locations inside the rotary kiln.

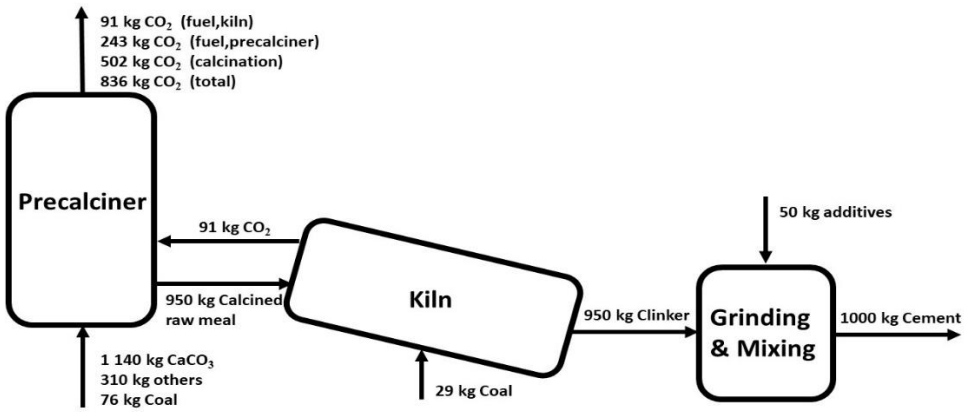

Figure 11: Sources of direct CO_2 emissions from CEM 1 cement manufacturing [138]

Hornberger et al. [139] experimentally studied a calcining reactor in an end-of-line calcium loop configuration for the capture of CO_2 from cement plants (see Figure 12). These authors stated that the calcium loop technology is considered to be particularly suitable for applications in the cement sector, since the clinker manufacturing process and calcium loop CO_2 capture process share a common raw material (i.e. $CaCO_3$), allowing for synergies such as the reuse of absorbents, the increase in make-up rates of the calcium loop system and the integration of energy. Li et al. [140] presented a study that compares CO_2 capture technologies for the cement manufacturing process and analyzed the economic and financial challenges of deploying CO_2 capture in the cement industry. Like Li et al. [140], De Lena et al. [143] used fluidized bed reactor technology to capture CO_2 from rotary kiln fumes. The technology proposed by De Lena et al. [143] consists of coupling the CFB oxy-fuel calciner in the circuit of the rotary kiln, to accomplish a dual purpose: (i) calcining the finest fraction of the raw meal to feed the plant's rotary kiln; and (ii) calcining the coarsest fraction of the fed raw meal, so as to recirculate part of it towards the carbonator as a means of capturing CO_2 from the kiln fumes. The results of this study indicate a reduction in equivalent CO_2 emissions of approximately 89-90%.

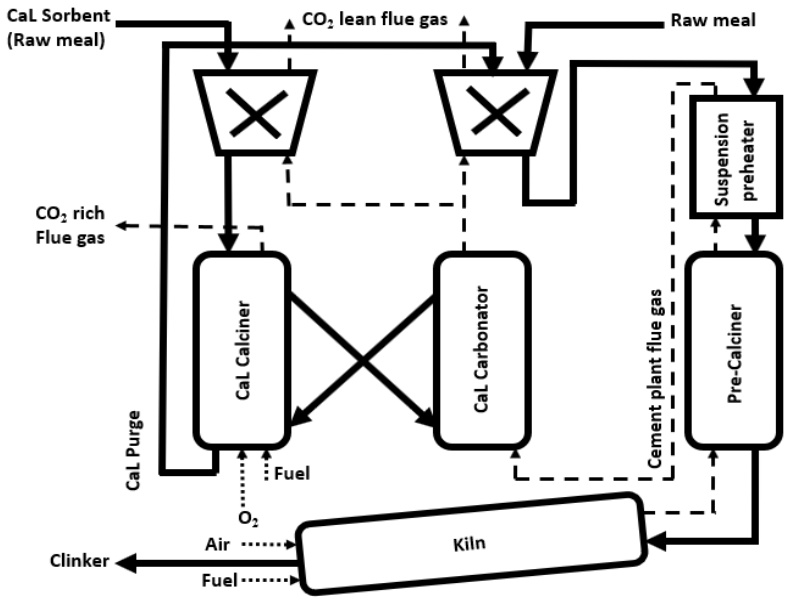

Figure 12: Tail-end calcium looping integration option for CO_2 capture from cement clinker production [139]

To better handle CO_2 emissions, Strunge et al. [144] proposed the CO_2 mineralization technology, whereby CO_2 is transformed into a thermodynamically stable carbonate. The authors claimed that such a technology is among the most promising. Napp et al. [145] focused on providing an overview of industrial process emission reduction technologies by compiling information from a wide range of sources. Liu et al. [146] worked on reducing CO emissions and reducing fluctuations in CO emitted during combustion, by introducing an oxygen-carrying material into the rotary kiln.

5.2. Energy optimization (recovery, storage and recovery of waste heat from the kiln, optimization of process control laws, etc.)

Given the limited resources available and faced with more stringent policies of ecological and energy transition, the cement plant with rotary kilns is being called upon to optimize its energy consumption. Energy optimization can be achieved in several ways: reduction of energy losses in the kiln circuits, by blocking all the vents and using high-performance refractory materials; reduction of unburnt matter (e.g. the presence of CO in the gas leaving the kiln) that still contains a certain amount of energy potentially usable in the process; control of the kiln burner and possibly the precalciner; and the use and recovery of materials similar to clinker, such as blast furnace slag and power station ash. The storage and recovery of heat waste from the kiln are keys to energy optimization. Huchet et al. [147] assessed an annular heat exchanger mounted on the external shell in order to recover the excess heat lost at the exterior wall of a rotary kiln. It is essential to establish methods and models for designing or controlling the process, in particular predictive control models, e.g. the Plant-Model Mismatch, to properly control the key process operating parameters. Teja et al. [148] presented a work on the control and optimization of a three-string cement rotary kiln using a predictive control model (PCM), with which they claimed that the PCM better handles disturbances, resulting in improved productivity, a reduction in energy consumption and the highest quality of finished product. Ramasamy et al. [149] proposed a work to determine the optimal PMM (Plant-Model Mismatch) parameters capable of improving PCM performance under various cement kiln operating scenarios. Stadler et al. [150] developed a predictive control model of a cement rotary kiln in the aim of controlling and optimizing clinker combustion in the cement production process. This model is based on the temperature profile control along the rotating cement kiln, in considering both convection and radiation transfers. Janati [151] developed an Aspen Plus process model and neural networks, which are able to accurately predict the energy efficiency of a cement rotary kiln. According to Teja et al. [148], the complex nature of cement kilns featuring longer time constants, changing raw material characteristics and nonlinear dynamics makes them very difficult to control; moreover, the

inclusion of various alternative fuels in combustion makes the process more complex since the fuel characteristics remain inconsistent throughout kiln operations.

5.3. Future trends in rotary kiln technology

The future trends of rotary kiln technology may focus on the use of completely decarbonized energy, whereby conventional and polluting fuels will be sidelined, in favor of a concentrating solar energy. A solar kiln avoids the traditional combustion of fossil fuels, which represents 40% of CO_2 emissions [11]. Thermal and thermochemical processes based on concentrating solar energy can also been combined with rotary kiln technology [152]. Concentrated solar power was introduced in rotary kilns in the 1950s [153]. Several authors argue about the ability of concentrated solar power to be able to provide high temperature renewable heat in any thermal industrial process [153–156]. Solar kilns would be able to overcome greenhouse gases issues, in particular CO_2, coming from the production of lime [154]. Neises et al. [157] worked on a solar-heated rotary kiln coupled with a solar kiln for the thermal reduction and oxidation of cobalt oxide. Moumin et al. [158] worked on the design and experimental evaluation of a high temperature solar rotary kiln dedicated to the calcination of raw cement. The calcination rate was found ranged between 24% and 99%, while the total efficiencies (thermal plus chemical) are ranged between 19% and 40%. However, the major challenge remains the intermittency of the solar source and the energy optimization of such kiln, which makes the application limited to pilot-scale applications. Most of the authors [152,153] argue about the importance of heat fluxes optimizing (gas suction, wall heat losses etc.) and reducing material conversion to increase the efficiency of the solar reactor. With regard to fine particle emissions, rotary kilns are being increasingly equipped with electro filters and/or high-precision dust collectors, capable of retaining a large portion of the particles present in the gas and preventing their escape into the chimney. CO_2 capture and sequestration technologies are still in the experimental phase, having not yet reached a stage of maturity; also, these technologies incur additional process energy costs.

6. Conclusion

The development of rotary kilns started in the second half of the 20^{th} century, largely due to the intensive production and quality control of cement during the clinkerization process. This article has sought to synthesize the physical mechanisms operating within these processes; such equipment has been applied to other types of materials of mineral or organic origin beyond its historical application. The thermochemical conversion of waste (e.g. biomass, tires) is just one example cited in this review (TiO_2, aluminum, asphalt aggregates, wood, coal pyrolysis). The underlying scientific problem, which remains a major obstacle, with this industrial process lies in its physical modeling. Indeed, several thousand particles coexist at the same time and are subjected to intense heat fluxes. Several chemical reactions take place, which lie at the origin of the endothermic and exothermic reactions responsible for various phase changes. General mass and energy balances for gas and solid phases therefore govern these complex physical processes. Their implementation is based on three scientific pillars, namely: (i) granular flow regimes and solid load control parameters, (ii) heat transport whether conductive, convective or radiative; and (iii) the kinetics reaction during the thermochemical conversion process.

From this overview, it has been shown that:

- The predictive models of the height or longitudinal profile of the solid load are similar in their geometric construction, being inspired by Seaman's original smooth drum model. Differences still need to be studied relative to more recent models. Let's note that a granular discharge model is to be implemented in the case of a flight rotary drum.
- No consensus has yet been forged for a model of mean residence time of the solid load despite the numerous experimental works established over the past few decades.
- Convective transfer models have been summarized (Gas-Solid, Gas-Wall, Wall-Exterior). These have provided a major contribution to the energy balance of the process. Work on this topic has progressed little, and correlations established for special cases are still being used.

- Conductive transfer models (Solid-Wall, Solid-Solid) are by and large currently presented as an effective law applicable to a bed of particles. Numerical tools at the grain scale (DEM, kinetic theory), coupled with continuous models at the furnace scale (CFD, reduced model), have started to be deployed in the scientific community to estimate the contribution of these collisions to the transfers.
- The existing radiative transfer models (Gas-Solid, Gas-Wall, Solid-Wall) are well referenced and contribute mainly to the energy balance. They are based on CFD work carried out on burners operating with fuel oil or natural gas. It is possible to estimate their contributions only if the emissivity of the surfaces involved can be measured.
- Transfers to the external environment of a convective and radiative nature can be accurately estimated if the experimental parameters are controlled (emissivity of the exterior wall and meteorological conditions).
- The reaction kinetics of an exothermic nature for clinkerization can be approximated by means of three sub-models (solid, gas, kiln wall) or from a 5-reaction model linking calcination, endothermic melting and exothermic clinkerization.
- For other applications, the basic theory of rotary kiln operations remains unchanged; however, new sub-models are required to obtain a reliable simulation.

In perspective, this paper has exposed the several potential paths to the scientific community devoted to the use of rotary kiln process in the present energy harvesting context. Alternative technologies are currently studied for gases management including dust emissions reduction (oxy-combustion, pyrolysis of alternative fuels) and CO_2 valorization. Optimal command laws, recovery/transport and storage of the heat waste remain the mains optimization tools.

List of abbreviations and symbols.

Latin letters

Symbol	Signification	Unit
A	cross-section	m^2
A_{wall}^{c}	surface of the wall covered by the bed	m^2
Bd	ratio of two speeds	-
Cp	specific heat capacity	J/kg/K
$\rho \times C_p$	volumetric heat capacity	$J/m^3/K$
d_p	particle diameter	m
D_{bed}	thermal diffusivity of the bed	m^2/s
$d_{kiln-in}$	inside diameter of the rotary kiln	m
D_{kiln}	external kiln diameter	m
D_h	hydraulic diameter of the kiln	m
E_{gas}	illumination	W/m^2
f	filling degree of the kiln	%
F_{B-gas}	bed- freeboard gas form factor	-
G_c	mass flow rate	kg/s
Gr	Grashof dimensionless number	-
h	coefficient of heat transfer	$W/m^2/K$
H_{bed}	height of the bed	m
J_{bed}	radiosity of the bed	W/m^2
l_{arc}	arc length of the material in contact with the kiln wall	m
L_{kiln}	length of kiln	m

M_c	mass of granular material	kg
n_{kiln}	speed of rotation of the kiln	tr/s
Nu	Nusselt dimensionless number	-
Pr	Prandtl dimensionless number	-
q_m	mass flow rate	kg/s
Re	Reynolds dimensionless number	-
Re_D	axial Reynolds number	-
Re_ω	angular Reynolds number	-
r_{kiln}	kiln radius	m
T	temperature	K
t_c	contact time between the wall and the particles	s
T_{gasFB}	freeboard gas temperature	K
V_a	axial velocity of the solid in a fully filled kiln ($V_a = q_m/(\rho_s \times \pi \times r_{kiln}^2)$)	m/s
V_k	maximum tangential velocity of the solid near the inner wall ($V_k = 2 \times \pi \times r_{kiln} \times n_{kiln}$).	m/s

Greek letters

α_g	absorptivity of freeboard gas	-
δ_{kiln}	kiln slope	degree
δ_{bed}	interception angle of the bed	degree
η	volume filling rate of the kiln	-
λ	thermal conductivity of the bed	W/m/K
ρ	bulk density	kg/m^3
σ_B	Stefan-Boltzmann's constant	W/m^2/K^4
φ_{bed}	angle of repose	degree
χ_{exp}	experimental constant (takes values between 0.1- 0.2)	-
χ_{ks}	dimensionless thickness of the air film surrounding the particles ($\chi_{ks} = 0.012$)	-
ψ	coefficients with grey body hypothesis	-
ω	angular velocity	rad/s

Subscripts

bed	solid bed of materials
$gas\ or\ g$	gas
$gasFB - B$	freeboard gas to solid bed of materials
$wall - B$	kiln wall to solid bed of materials
$gasFB - W$	freeboard gas to kiln wall
$wall$	wall

Superscripts

Rad	radiation
ext	exterior
$Conv$	convection
$Cond$	conduction

References

[1] A.A. Boateng, P.V. Barr, A thermal model for the rotary kiln including heat transfer within the bed, Int J Heat Mass Transf. 39 (1996) 2131–2147.
[2] F.M. Lea, P.C. Hewlett, Lea's chemistry of cement and concrete, 4th ed, Arnold ; Copublished in North, Central, and South America by J. Wiley, London : New York, 1998.
[3] G.R. Redgrave Spackman, Charles,, Calcareous cements: their nature, manufacture, and uses., C. Griffin and Company, Limited, London, 1924.
[4] A.C. Davis, A hundred years of Portland cement, 1824-1924, Concrete Publications Ltd., London, 1924.
[5] K.E. Peray, The rotary cement kiln, Chemical Pub. Co., New York, 1986.
[6] M. Debacq, S. Vitu, D. Ablitzer, J.-L. Houzelot, F. Patisson, Transverse motion of cohesive powders in flighted rotary kilns: experimental study of unloading at ambient and high temperatures, Powder Technol. 245 (2013) 56–63. https://doi.org/10.1016/j.powtec.2013.04.007.
[7] J. Seidenbecher, F. Herz, C. Meitzner, E. Specht, S. Wirtz, V. Scherer, X. Liu, Experimental analysis of the flight design effect on the temperature distribution in rotary kilns, Chem. Eng. Sci. 240 (2021) 116652. https://doi.org/10.1016/j.ces.2021.116652.
[8] M. Piton, F. Huchet, O. Le Corre, L. Le Guen, B. Cazacliu, A coupled thermal-granular model in flights rotary kiln: Industrial validation and process design, Appl. Therm. Eng. 75 (2015) 1011–1021. https://doi.org/10.1016/j.applthermaleng.2014.10.052.
[9] N. Descoins, J.-L. Dirion, T. Howes, Solid transport in a pyrolysis pilot-scale rotary kiln: preliminary results—stationary and dynamic results, Pneum. Conveying Handl. Part. Solids. 44 (2005) 315–321. https://doi.org/10.1016/j.cep.2004.02.025.
[10] F. Marias, H. Roustan, A. Pichat, Modelling of a rotary kiln for the pyrolysis of aluminium waste, Chem. Eng. Sci. 60 (2005) 4609–4622. https://doi.org/10.1016/j.ces.2005.03.025.
[11] B.-J.R. Mungyeko Bisulandu, Modélisation de l'apport d'énergie par combustibles alternatifs dans les fours tournants de production de ciment, Université de Pau et des Pays de l'Adour, 2018. http://www.theses.fr/2018PAUU3001.
[12] A.A. Boateng, P.V. Barr, Modelling of particle mixing and segregation in the transverse plane of a rotary kiln, Chem. Eng. Sci. 51 (1996) 4167 4181.
[13] J. Mellmann, The transverse motion of solids in rotating cylinders—forms of motion and transition behavior, Powder Technol. 118 (2001) 251–270. https://doi.org/10.1016/S0032-5910(00)00402-2.
[14] H. Yin, M. Zhang, H. Liu, Numerical simulation of three-dimensional unsteady granular flows in rotary kiln, Powder Technol. 253 (2014) 138–145. https://doi.org/10.1016/j.powtec.2013.10.044.
[15] X.Y. Liu, E. Specht, J. Mellmann, Slumping–rolling transition of granular solids in rotary kilns, Chem. Eng. Sci. 60 (2005) 3629–3636. https://doi.org/10.1016/j.ces.2005.02.020.
[16] H. Yin, M. Zhang, H. Liu, Numerical simulation of three-dimensional unsteady granular flows in rotary kiln, Powder Technol. 253 (2014) 138–145. https://doi.org/10.1016/j.powtec.2013.10.044.
[17] H. Liu, H. Yin, M. Zhang, M. Xie, X. Xi, Numerical simulation of particle motion and heat transfer in a rotary kiln, Powder Technol. 287 (2016) 239–247. https://doi.org/10.1016/j.powtec.2015.10.007.
[18] P.J. Witt, M.D. Sinnott, P.W. Cleary, M.P. Schwarz, A hierarchical simulation methodology for rotary kilns including granular flow and heat transfer, Miner. Eng. 119 (2018) 244–262. https://doi.org/10.1016/j.mineng.2018.01.035.
[19] M. Saruwatari, H. Nakamura, Coarse-grained discrete element method of particle behavior and heat transfer in a rotary kiln, Chem. Eng. J. 428 (2022) 130969. https://doi.org/10.1016/j.cej.2021.130969.
[20] F. Cantelaube, D. Bideau, S. Roux, Kinetics of segregation of granular media in a two-dimensional rotating drum, Powder Technol. 93 (1997) 1–11. https://doi.org/10.1016/S0032-5910(97)03213-0.
[21] Z.S. Khan, S.W. Morris, Subdiffusive Axial Transport of Granular Materials in a Long Drum Mixer, Phys. Rev. Lett. 94 (2005) 048002. https://doi.org/10.1103/PhysRevLett.94.048002.

[22] A.S. Bongo Njeng, S. Vitu, M. Clausse, J.-L. Dirion, M. Debacq, Effect of lifter shape and operating parameters on the flow of materials in a pilot rotary kiln: Part III. Up-scaling considerations and segregation analysis, Powder Technol. 297 (2016) 415–428. https://doi.org/10.1016/j.powtec.2016.04.052.
[23] C. Beaulieu, D. Vidal, F. Bertrand, J. Chaouki, Impact of granular segregation on heat transfer in horizontal drums, Chem. Eng. J. 409 (2021) 128039. https://doi.org/10.1016/j.cej.2020.128039.
[24] B. Yari, C. Beaulieu, P. Sauriol, F. Bertrand, J. Chaouki, Size segregation of bidisperse granular mixtures in rotating drum, Powder Technol. 374 (2020) 172–184. https://doi.org/10.1016/j.powtec.2020.07.030.
[25] A.A. Boateng, Rotary kilns-Transport Phenomena and Transport Processes, United States of America, 2012.
[26] H. Kramers, P. Croockewit, The passage of granular solids through inclined rotary kilns, Chem. Eng. Sci. 1 (1952) 259–265. https://doi.org/10.1016/0009-2509(52)87019-8.
[27] W.-N. Wu, X.-Y. Liu, Z. Hu, F. Herz, E. Specht, Measurement of the local material depth in a directly-heated pilot rotary kiln based on temperature fields, Powder Technol. 330 (2018) 12–18. https://doi.org/10.1016/j.powtec.2018.02.005.
[28] K.S. Mujumdar, V.V. Ranade, Simulation of Rotary Cement Kilns Using a One-Dimensional Model, Chem. Eng. Res. Des. 84 (2006) 165–177. https://doi.org/10.1205/cherd.04193.
[29] E. Specht, Y.-C. Shi, H. Woche, J. Knabbe, U. Sprinz, Experimental investigation of solid bed depth at the discharge end of rotary kilns, Powder Technol. 197 (2010) 17–24. https://doi.org/10.1016/j.powtec.2009.08.024.
[30] P.R. Davies, M.J.S. Norton, D.I. Wilson, J.F. Davidson, D.M. Scott, Gas flow in rotary kilns, Particuology. 8 (2010) 613–616. https://doi.org/10.1016/j.partic.2010.07.014.
[31] D.A. Granados, F. Chejne, J.M. Mejía, C.A. Gómez, A. Berrío, W.J. Jurado, Effect of flue gas recirculation during oxy-fuel combustion in a rotary cement kiln, Energy. 64 (2014) 615–625. https://doi.org/10.1016/j.energy.2013.09.045.
[32] X.Y. Liu, E. Specht, Mean residence time and hold-up of solids in rotary kilns, Chem. Eng. Sci. 61 (2006) 5176–5181. https://doi.org/10.1016/j.ces.2006.03.054.
[33] M. Debacq, P. Thammavong, S. Vitu, D. Ablitzer, J.-L. Houzelot, F. Patisson, A hydrodynamic model for flighted rotary kilns used for the conversion of cohesive uranium powders, Chem. Eng. Sci. 104 (2013) 586–595. https://doi.org/10.1016/j.ces.2013.09.037.
[34] X.Y. Liu, J. Zhang, E. Specht, Y.C. Shi, F. Herz, Analytical solution for the axial solid transport in rotary kilns, Chem. Eng. Sci. 64 (2009) 428–431. https://doi.org/10.1016/j.ces.2008.10.024.
[35] S. Ngako, R. Mouangue, S. Caillat, A. Kuitche, E. Saragba, Numerical investigation of bed depth height, axial velocity and mean residence time of inert particles in steady state industrial cement rotary kiln: Case of Figuil Plant in Cameroon, Powder Technol. 271 (2015) 221–227. https://doi.org/10.1016/j.powtec.2014.11.007.
[36] W.C. Saeman, Passage of solids through rotary kilns, Chem Eng Prog. 47 (1951) 508–514.
[37] L. Vàhl, W.G. Kingma, Transport of solids through horizontal rotary cylinders, Chem. Eng. Sci. 1 (1952) 253–258.
[38] B. Colin, Modélisation de la torréfaction de plaquettes de bois en four tournant et validation expérimentale à l'échelle d'un pilote continu de laboratoire, Université de Toulouse, Albi-carmaux & INP Toulouse, 2014.
[39] T. Haeldermans, M.A. Lataf, G. Vanroelen, P. Samyn, D. Vandamme, A. Cuypers, K. Vanreppelen, S. Schreurs, Numerical prediction of the mean residence time of solid materials in a pilot-scale rotary kiln, Powder Technol. 354 (2019) 392–401. https://doi.org/10.1016/j.powtec.2019.06.008.
[40] J.D. Sullivan, C.G. Maier, O.C. Ralston, Passage of solid particles through rotary cylindrical kilns, Govt. Print. Off., Washington, 1927.
[41] A. Chatterjee, A.V. Sathe, P.K. Mukhopadhyay, Flow of materials in rotary kilns used for sponge iron manufacture: Part II. Effect of kiln geometry, Metall. Trans. B. 14 (1983) 383–392. https://doi.org/10.1007/BF02654357.

[42] D.W. Green, R.H. Perry, Perry's Chemical Engineers' Handbook, Eighth Edition, 8th ed. /, McGraw-Hill Education, New York, 2008. https://www.accessengineeringlibrary.com/content/book/9780071422949.
[43] A. Donatelli, P. Garzone, P. Iovane, Discharging granular material from a rotary kiln in a slumping regime: Theoretical and experimental studies, Particuology. 23 (2015) 56–61. https://doi.org/10.1016/j.partic.2015.02.003.
[44] C.C. Lee, S. Lin, eds., Handbook of environmental engineering calculations, McGraw-Hill, New York, 2000.
[45] J. Perron, R.T. Bui, Rotary cylinders: Solid transport prediction by dimensional and rheological analysis, Can. J. Chem. Eng. 68 (1990) 61–68. https://doi.org/10.1002/cjce.5450680108.
[46] D.M. Scott, J.F. Davidson, S.-Y. Lim, R.J. Spurling, Flow of granular material through an inclined, rotating cylinder fitted with a dam, Powder Technol. 182 (2008) 466–473. https://doi.org/10.1016/j.powtec.2007.07.017.
[47] M. Danish, S. Kumar, S. Kumar, Exact analytical solution for the bed depth profile of solids flowing in a rotary kiln, Powder Technol. 230 (2012) 29–35. https://doi.org/10.1016/j.powtec.2012.06.042.
[48] Z. Zhang, Y. Wu, H. Li, X. Li, X. Gao, A simple step-change method to determine mean residence time in rotary kiln and a predictive model at low inclination, Powder Technol. 333 (2018) 30–37. https://doi.org/10.1016/j.powtec.2018.04.002.
[49] N. Parveen, S. Zaidi, M. Danish, Development and analyses of data-driven models for predicting the bed depth profile of solids flowing in a rotary kiln, Adv. Powder Technol. 31 (2020) 678–694. https://doi.org/10.1016/j.apt.2019.11.023.
[50] L.G. Ndiaye, S. Caillat, A. Chinnayya, D. Gambier, B. Baudoin, Application of the dynamic model of Saeman to an industrial rotary kiln incinerator: Numerical and experimental results, Waste Manag. 30 (2010) 1188–1195. https://doi.org/10.1016/j.wasman.2009.09.023.
[51] J. Zheng, L. Zhao, W. Du, Hybrid model of a cement rotary kiln using an improved attention-based recurrent neural network, ISA Trans. 129 (2022) 631–643. https://doi.org/10.1016/j.isatra.2022.02.018.
[52] P.J. Witt, J. Johnson, M.P. Schwarz, An efficient method for computational flow-based simulation of heat transfer in a rotary kiln with pilot scale validation, Appl. Therm. Eng. 214 (2022) 118894. https://doi.org/10.1016/j.applthermaleng.2022.118894.
[53] A. Gallo, E. Alonso, C. Pérez-Rábago, E. Fuentealba, M.I. Roldán, A lab-scale rotary kiln for thermal treatment of particulate materials under high concentrated solar radiation: Experimental assessment and transient numerical modeling, Sol. Energy. 188 (2019) 1013–1030. https://doi.org/10.1016/j.solener.2019.07.006.
[54] A. Cholette, L. Cloutier, Mixing efficiency determinations for continuous flow systems, Can. J. Chem. Eng. 37 (1959) 105–112. https://doi.org/10.1002/cjce.5450370305.
[55] F. Mintus, S. Hamel, W. Krumm, Wet process rotary cement kilns: modeling and simulation, Clean Techn Env. Policy. (2006) 112–122. https://doi.org/10.1007/s10098-006-0039-6.
[56] J. Lasek, K. Głód, K. Słowik, A. Cygan, Y.-H. Li, Static and dynamic characteristics of rotary kiln reactor during processing of biomass and municipal solid waste, Powder Technol. 404 (2022) 117476. https://doi.org/10.1016/j.powtec.2022.117476.
[57] M. Renaud, J. Thibault, A. Trusiak, Solids transportation model of an industrial rotary dryer, Dry. Technol. 18 (2000) 843–865. https://doi.org/10.1080/07373930008917741.
[58] E. Alonso, A. Gallo, M.I. Roldán, C.A. Pérez-Rábago, E. Fuentealba, Use of rotary kilns for solar thermal applications: Review of developed studies and analysis of their potential, Sol. Energy. 144 (2017) 90–104. https://doi.org/10.1016/j.solener.2017.01.004.
[59] H. Henein, J.K. Brimacombe, A.P. Watkinson, An experimental study of segregation in rotary kilns, Metall. Trans. B. 16 (1985) 763–774. https://doi.org/10.1007/BF02667512.
[60] Y. Demagh, H. Ben Moussa, M. Lachi, S. Noui, L. Bordja, Surface particle motions in rotating cylinders: Validation and similarity for an industrial scale kiln, Powder Technol. 224 (2012) 260–272. https://doi.org/10.1016/j.powtec.2012.03.002.
[61] A.V. Orpe, D.V. Khakhar, Scaling relations for granular flow in quasi-two-dimensional rotating cylinders, Phys. Rev. E. 64 (2001) 031302. https://doi.org/10.1103/PhysRevE.64.031302.

[62] M.M.H.D. Arntz, H.H. Beeftink, W.K. den Otter, W.J. Briels, R.M. Boom, Segregation of granular particles by mass, radius, and density in a horizontal rotating drum, AIChE J. 60 (2014) 50–59. https://doi.org/10.1002/aic.14241.
[63] N. Jain, J.M. Ottino, R.M. Lueptow, Regimes of segregation and mixing in combined size and density granular systems: an experimental study, Granul. Matter. 7 (2005) 69–81. https://doi.org/10.1007/s10035-005-0198-x.
[64] D.R. Van Puyvelde, Simulating the mixing and segregation of solids in the transverse section of a rotating kiln, Powder Technol. 164 (2006) 1–12. https://doi.org/10.1016/j.powtec.2005.12.017.
[65] T. Ginsberg, M. Modigell, Dynamic modelling of a rotary kiln for calcination of titanium dioxide white pigment, Comput. Chem. Eng. 35 (2011) 2437–2446. https://doi.org/10.1016/j.compchemeng.2011.03.029.
[66] G.J. Thornton, R.J. Batterham, The transfer of heat in kilns, Proc CHEMECA 82 Natl. Conf. Publ. No 829. (1982) 260–266.
[67] J.P. Gorog, J.K. Brimacombe, T.N. Adams, Radiative heat transfer in rotary kilns, Metall. Trans. B. 12 (1981) 55–70. https://doi.org/10.1007/BF02674758.
[68] J.A. Thurlby, A dynamic mathematical model of the complete grate/kiln iron–ore pellet induration process, Metall. Trans. B. 19 (1988) 103–112. https://doi.org/10.1007/BF02666496.
[69] A.R. Nielsen, Combustion of large solid fuels in cement rotary kilns: Ph.D. Thesis, Department of Chemistry, Technical University of Denmark, Kgs. Lyngby, 2012. http://www.forskningsdatabasen.dk/en/catalog/2185763052.
[70] A. Atmaca, R. Yumrutaş, Thermodynamic and exergoeconomic analysis of a cement plant: Part II – Application, Energy Convers. Manag. 79 (2014) 799–808. https://doi.org/10.1016/j.enconman.2013.11.054.
[71] A. Atmaca, R. Yumrutas, Thermodynamic and exergoeconomic analysis of a cement plant: Part I – Methodology, Energy Convers. Manag. (2014) 790–798.
[72] E. Tsotsas, Particle-particle heat transfer in thermal DEM: Three competing models and a new equation, Int. J. Heat Mass Transf. 132 (2019) 939–943. https://doi.org/10.1016/j.ijheatmasstransfer.2018.12.090.
[73] F. Hanrot, Analyse physico-chimique et modélisation de la pyrolyse de grains de charbon en four tournant, Institut National Polytechnique de Lorraine-INPL, 1992.
[74] C. Csernyei, A.G. Straatman, Numerical modeling of a rotary cement kiln with improvements to shell cooling, Int. J. Heat Mass Transf. 102 (2016) 610–621. https://doi.org/10.1016/j.ijheatmasstransfer.2016.06.058.
[75] S.H. Tscheng, A.P. Watkinson, Convective heat transfer in a rotary kiln, Can. J. Chem. Eng. 57 (1979) 433–443.
[76] E. Mastorakos, A. Massias, C.D. Tsakiroglou, D.A. Goussis, V.N. Burganos, A.C. Payatakes, CFD predictions for cement kilns including Flame modelling, heat transfer and clinker chemistry, (1999) 55–76.
[77] P.V. Barr, J.K. Brimacombe, A.P. Watkinson, A heat-transfer model for the rotary kiln: Part II. Development of the cross-section model, Metall. Trans. B. 20 (1989) 403–419.
[78] P. Lybaert, Contribution à l'étude du transfert de chaleur entre un matériau particulaire et la paroi dans les échangeurs rotatifs indirects, Faculté Polytechnique de Mons, 1985.
[79] A. Agrawal, P.S. Ghoshdastidar, Numerical simulation of heat transfer during production of rutile titanium dioxide in a rotary kiln, Int. J. Heat Mass Transf. 106 (2017) 263–279. https://doi.org/10.1016/j.ijheatmasstransfer.2016.10.024.
[80] D. Shi, W.L. Vargas, J.J. McCarthy, Heat transfer in rotary kilns with interstitial gases, Chem. Eng. Sci. 63 (2008) 4506–4516. https://doi.org/10.1016/j.ces.2008.06.006.
[81] E. Specht, Heat and mass transfer in thermoprocessing: fundamentals, calculations, processes, 1st edition, Vulkan Verlag, Essen, Germany, 2017.
[82] W.N. Sullivan, R.H. Sabersky, Heat transfer to flowing granular media, Int. J. Heat Mass Transf. 18 (1975) 97–107. https://doi.org/10.1016/0017-9310(75)90012-5.
[83] S.-Q. Li, L.-B. Ma, W. Wan, Q. Yao, A Mathematical Model of Heat Transfer in a Rotary Kiln Thermo-Reactor, Chem. Eng. Technol. 28 (2005) 1480–1489. https://doi.org/10.1002/ceat.200500241.

[84] M.U. Babler, A. Phounglamcheik, M. Amovic, R. Ljunggren, K. Engvall, Modeling and pilot plant runs of slow biomass pyrolysis in a rotary kiln, Appl. Energy. (2017). https://doi.org/10.1016/j.apenergy.2017.06.034.
[85] G.W.J. Wes, A.A.H. Drinkenburg, S. Stemerding, Heat transfer in a horizontal rotary drum reactor, Powder Technol. 13 (1976) 185–192. https://doi.org/10.1016/0032-5910(76)85003-6.
[86] F. Huchet, L. Le Guen, P. Richard, M. Piton, B. Cazacliu, P. Semelle, J. Matheus, H. Riche, P. Tamagny, Influence of asphalt composition upon the thermodynamics performance of a mixing plant, Road Mater. Pavement Des. 19 (2016) 104–119. https://doi.org/10.1080/14680629.2016.1249018.
[87] M. Piton, F. Huchet, O. Le Corre, L. Le Guen, B. Cazacliu, A coupled thermal-granular model in flights rotary kiln: Industrial validation and process design, Appl. Therm. Eng. 75 (2015) 1011–1021. https://doi.org/10.1016/j.applthermaleng.2014.10.052.
[88] X. Fan, J. Li, X. Chen, Y. Wang, M. Gan, Temperature Field Simulation Model for Rotary Kiln of Iron Ore Oxidized Pellet, J. Iron Steel Res. Int. 20 (2013) 16–19. https://doi.org/10.1016/S1006-706X(13)60076-X.
[89] E. Lebas, Etude et modélisation de la pyrolyse du charbon en four tournant, Institut National Polytechnique de Lorraine-INPL, 1995.
[90] H. Liu, H. Yin, M. Zhang, M. Xie, X. Xi, Numerical simulation of particle motion and heat transfer in a rotary kiln, Powder Technol. 287 (2016) 239–247. https://doi.org/10.1016/j.powtec.2015.10.007.
[91] U. Küssel, D. Abel, M. Schumacher, M. Weng, Modeling of Rotary Kilns and Application to Limestone Calcination, in: 2009: pp. 814–822. https://doi.org/10.3384/ecp09430084.
[92] A. Gunnarsson, K. Andersson, B.R. Adams, C. Fredriksson, Full-scale 3D-modelling of the radiative heat transfer in rotary kilns with a present bed material, Int. J. Heat Mass Transf. 147 (2020) 118924.
[93] J.P. Gorog, T.N. Adams, J.K. Brimacombe, Regenerative heat transfer in rotary kilns, Metall. Trans. B. 13 (1982) 153–163.
[94] Engineering toolbox, Dry Air Properties, Httpwwwengineeringtoolboxcomdry-Air-Prop.-D973html. (2017).
[95] H. Hausen, Wärmeübertragung im Gegenstrom, Gleichstrom und Kreuzstrom, Springer Berlin Heidelberg, 2013. https://books.google.fr/books?id=ArnPBgAAQBAJ.
[96] H. Hausen, Darstellung des warmeuberganges in rohren durch verallge-meinerte potenzbeziehungen, Z VDI Beih. Verfahrenstechnik 4 91. 4 (1943) 91–98.
[97] M. Piton, Récupération de la chaleur fatale: application aux fours rotatifs, Nantes, Ecole des Mines, 2015. http://www.theses.fr/2015EMNA0235 (accessed August 22, 2017).
[98] S. Seghir-Ouali, D. Saury, S. Harmand, O. Phillipart, D. Laloy, Convective heat transfer inside a rotating cylinder with an axial air flow, Int. J. Therm. Sci. 45 (2006) 1166–1178. https://doi.org/10.1016/j.ijthermalsci.2006.01.017.
[99] J.B. Riffaud, B. Koehret, Modeling and simulation of an alumina kiln, Brit Chem Eng Proc Tech. 17 (1972) 413–419.
[100] J. Li, D.J. Mason, A computational investigation of transient heat transfer in pneumatic transport of granular particles, Powder Technol. 112 (2000) 273–282. https://doi.org/10.1016/S0032-5910(00)00302-8.
[101] L. Le Guen, M. Piton, Q. Hénaut, F. Huchet, P. Richard, Heat convection and radiation in flighted rotary kilns: A minimal model, Can. J. Chem. Eng. 95 (2017) 100–110. https://doi.org/10.1002/cjce.22659.
[102] L.K. Nørskov, Combustion of solid alternative fuels in the cement kiln burner, Technical University of Denmark, 2012. http://www.forskningsdatabasen.dk/en/catalog/2185752638 (accessed June 5, 2017).
[103] J. Chang, G. Wang, J. Gao, K. Zhang, H. Chen, Y. Yang, CFD modeling of particle–particle heat transfer in dense gas-solid fluidized beds of binary mixture, Powder Technol. 217 (2012) 50–60. https://doi.org/10.1016/j.powtec.2011.10.008.

[104] J. Felinks, S. Richter, B. Lachmann, S. Brendelberger, M. Roeb, C. Sattler, R. Pitz-Paal, Particle–particle heat transfer coefficient in a binary packed bed of alumina and zirconia-ceria particles, Appl. Therm. Eng. 101 (2016) 101–111. https://doi.org/10.1016/j.applthermaleng.2016.01.066.
[105] J. Chang, S. Yang, K. Zhang, A particle-to-particle heat transfer model for dense gas–solid fluidized bed of binary mixture, Chem. Eng. Res. Des. 89 (2011) 894–903. https://doi.org/10.1016/j.cherd.2010.08.004.
[106] N. Gui, J. Yan, W. Xu, L. Ge, D. Wu, Z. Ji, J. Gao, S. Jiang, X. Yang, DEM simulation and analysis of particle mixing and heat conduction in a rotating drum, Chem. Eng. Sci. 97 (2013) 225–234. https://doi.org/10.1016/j.ces.2013.04.005.
[107] P.V. Barr, J.K. Brimacombe, A.P. Watkinson, A heat-transfer model for the rotary kiln: Part I. pilot kiln trials, Metall. Trans. B. 20 (1989) 391–402.
[108] A.P. Watkinson, J.K. Brimacombe, Heat Transfer in a Direct-Fired Rotary Kiln: I. Pilot plant and experimentation, Metall. Trans. B. VOLUME 9B (1978) 201–208.
[109] E.-U. Schlünder, N. Mollekopf, Vacuum contact drying of free flowing mechanically agitated particulate material, Chem. Eng. Process. Process Intensif. 18 (1984) 93–111. https://doi.org/10.1016/0255-2701(84)85012-6.
[110] B.-J.R. Mungyeko Bisulandu, F. Marias, Modeling of the Thermochemical Conversion of Biomass in Cement Rotary Kiln, Waste Biomass Valor. 12 (2021) 1005–1024. https://doi.org/10.1007/s12649-020-01001-9.
[111] J. Lehmberg, M. Hehl, K. Schügerl, Transverse mixing and heat transfer in horizontal rotary drum reactors, Powder Technol. 18 (1977) 149–163. https://doi.org/10.1016/0032-5910(77)80004-1.
[112] V. Gnielinski, Neue Gleichungen für den Wärme- und den Stoffübergang in turbulent durchströmten Rohren und Kanälen, Forsch. Im Ingenieurwesen A. 41 (1975) 8–16. https://doi.org/10.1007/BF02559682.
[113] D. Machalek, K.M. Powell, Model predictive control of a rotary kiln for fast electric demand response, Miner. Eng. 144 (2019) 106021. https://doi.org/10.1016/j.mineng.2019.106021.
[114] J. Urbano, J. Henriquez, A. Ochoa, A. Primo, B. Souza, Dynamic modeling of the heat transfer process in rotary kilns with indirect oil heating: Parametric analysis of gypsum calcination case, Therm. Sci. 26 (2022) 1637–1648. https://doi.org/10.2298/TSCI210523245U.
[115] M.N. Özışık, Heat transfer: a basic approach, McGraw-Hill, New York, 1985.
[116] J. Sucec, Heat Transfer Data Book, Simon&Schuster, New York, 1975.
[117] W.M. Kays, J.S. Bjorklund, Heat transfer from a rotating cylinder with and without crossflow, Trans ASME. 80C (1958) 70–78.
[118] L. Labraga, T. Berkah, Mass transfer from a rotating cylinder with and without crossflow, 47 (2004) 2493–2499.
[119] H.C. Hottel, A.F. Sarofim, Radiative Transfer, 1st edition, McGraw-Hill, New York, USA, 1967.
[120] P.V. Barr, Heat transfer processes in rotary kilns, Ph D Thesis, University of British Columbia, 1986.
[121] A. Manitius, E. Kurcyusz, W. Kawecki, Mathematical Model of the Aluminium Oxide Rotary Kiln, IEC Proc Dev. (1974) 132–142.
[122] W.K.H. Ariyaratne, A. Malagalage, M.C. Melaaen, L.-A. Tokheim, CFD modelling of meat and bone meal combustion in a cement rotary kiln – Investigation of fuel particle size and fuel feeding position impacts, Chem. Eng. Sci. 123 (2015) 596–608. https://doi.org/10.1016/j.ces.2014.10.048.
[123] H.A. Spang, A dynamic model of a cement kiln, Automatica. 8 (1972) 309–323. https://doi.org/10.1016/0005-1098(72)90050-7.
[124] S. Wang, J. Lu, W. Li, J. Li, Z. Hu, Modeling of Pulverized Coal Combustion in Cement Rotary Kiln, Energy Fuels. 20 (2006) 2350–2356. https://doi.org/10.1021/ef060027p.
[125] W.K. Hiromi Ariyaratne, E.V.P.J. Manjula, M.C. Melaaen, L.-A. Tokheim, Mathematical Model for Alternative Fuel Combustion in a Rotary Cement Kiln Burner, Int. J. Model. Optim. 4 (2014) 56–61. https://doi.org/10.7763/IJMO.2014.V4.347.

[126] T.P. Bhad, S. Sarkar, A. Kaushik, S.V. Herrwardkar, CFD Modeling of a cement Kiln with multi channel burner for optimization of flame profile, in: Proc. Seventh Int. Conf. CFD Miner. Process Ind., 2009. http://www.cfd.com.au/cfd_conf09/PDFs/048SAR.pdf (accessed February 12, 2016).
[127] P. Darabi, A mathematical model for cement kilns, University of British Columbia, 2007.
[128] U. Kaantee, R. Zevenhoven, R. Backman, M. Hupa, Cement manufacturing using alternative fuels and the advantages of process modelling, Fuel Process. Technol. 85 (2004) 293–301. https://doi.org/10.1016/S0378-3820(03)00203-0.
[129] B. Colin, J.-L. Dirion, P. Arlabosse, S. Salvador, Wood chips flow in a rotary kiln: Experiments and modeling, Chem. Eng. Res. Des. 98 (2015) 179–187. https://doi.org/10.1016/j.cherd.2015.04.017.
[130] F. Marias, A model of a rotary kiln incinerator including processes occurring within the solid and the gaseous phases, Comput. Chem. Eng. 27 (2003) 813–825. https://doi.org/10.1016/S0098-1354(02)00268-5.
[131] L. Le Guen, F. Huchet, Thermal imaging as a tool for process modelling: application to a flight rotary kiln, Quant. InfraRed Thermogr. J. 17 (2020) 79–95. https://doi.org/10.1080/17686733.2019.1611222.
[132] L. Le Guen, F. Huchet, J. Dumoulin, A wall heat transfer correlation for the baffled-rotary kilns with secondary air flow and recycled materials inlet, Exp. Therm. Fluid Sci. 54 (2014) 110–116. https://doi.org/10.1016/j.expthermflusci.2014.01.020.
[133] M. Gürtürk, H.F. Oztop, Energy and exergy analysis of a rotary kiln used for plaster production, Appl. Therm. Eng. 67 (2014) 554–565. https://doi.org/10.1016/j.applthermaleng.2014.03.025.
[134] K.R. Sunkara, F. Herz, E. Specht, J. Mellmann, Influence of flight design on the particle distribution of a flighted rotating drum, Chem. Eng. Sci. 90 (2013) 101–109. https://doi.org/10.1016/j.ces.2012.12.035.
[135] E. Zwolińska, V. Gogulancea, Y. Sun, V. Lavric, A. Chmielewski, A kinetic sensitivity analysis for the SO 2 and NO x removal using the electron beam technology, Radiat. Phys. Chem. 138 (2017) 29–36. https://doi.org/10.1016/j.radphyschem.2017.05.004.
[136] F. Marias, J.-R. Puiggali, Simulation numérique d'un brûleur industriel. Analyse qualitative des effets de swirl sur l'écoulement et sur la production de polluants, Int. J. Therm. Sci. 39 (2000) 249–264. https://doi.org/10.1016/S1290-0729(00)00243-X.
[137] U.C. Mishra, S. Sarsaiya, A. Gupta, A systematic review on the impact of cement industries on the natural environment, Environ. Sci. Pollut. Res. (2022). https://doi.org/10.1007/s11356-022-18672-7.
[138] T. Hills, N. Florin, P.S. Fennell, Decarbonising the cement sector: A bottom-up model for optimising carbon capture application in the UK, J. Clean. Prod. 139 (2016) 1351–1361. https://doi.org/10.1016/j.jclepro.2016.08.129.
[139] M. Hornberger, J. Moreno, M. Schmid, G. Scheffknecht, Experimental investigation of the calcination reactor in a tail-end calcium looping configuration for CO2 capture from cement plants, Fuel. 284 (2021) 118927. https://doi.org/10.1016/j.fuel.2020.118927.
[140] J. Li, P. Tharakan, D. Macdonald, X. Liang, Technological, economic and financial prospects of carbon dioxide capture in the cement industry, Energy Policy. 61 (2013) 1377–1387. https://doi.org/10.1016/j.enpol.2013.05.082.
[141] M. Hornberger, J. Moreno, M. Schmid, G. Scheffknecht, Experimental investigation of the carbonation reactor in a tail-end Calcium Looping configuration for CO2 capture from cement plants, Fuel Process. Technol. 210 (2020) 106557. https://doi.org/10.1016/j.fuproc.2020.106557.
[142] Ö. Mutlu, P. Roy, T. Zeng, Downstream Torrefaction of Wood Pellets in a Rotary Kiln Reactor—Impact on Solid Biofuel Properties and Torr-Gas Quality, Processes. 10 (2022) 1912. https://doi.org/10.3390/pr10101912.
[143] E. De Lena, B. Arias, M.C. Romano, J.C. Abanades, Integrated Calcium Looping System with Circulating Fluidized Bed Reactors for Low CO2 Emission Cement Plants, Int. J. Greenh. Gas Control. 114 (2022) 103555. https://doi.org/10.1016/j.ijggc.2021.103555.
[144] T. Strunge, H. Naims, H. Ostovari, B. Olfe-Kräutlein, Priorities for supporting emission reduction technologies in the cement sector – A multi-criteria decision analysis of CO2

mineralisation, J. Clean. Prod. 340 (2022) 130712. https://doi.org/10.1016/j.jclepro.2022.130712.
[145] T.A. Napp, A. Gambhir, T.P. Hills, N. Florin, P.S. Fennell, A review of the technologies, economics and policy instruments for decarbonising energy-intensive manufacturing industries, Renew. Sustain. Energy Rev. 30 (2014) 616–640. https://doi.org/10.1016/j.rser.2013.10.036.
[146] X. Liu, L. Duan, Y. Duan, L. Li, Z. Sun, G. Sun, Improved fuel conversion through oxygen carrier aided combustion during incineration of biomass-based solid waste in a rotary kiln, Fuel. 331 (2023) 125714. https://doi.org/10.1016/j.fuel.2022.125714.
[147] F. Huchet, M. Piton, A. Del Barrio, O. Le Corre, B. Cazacliu, Air-cooling heat exchanger applied to external rotary kiln wall in forced and natural draft, Energy Convers. Manag. 154 (2017) 517–525.
[148] R. Teja, P. Sridhar, M. Guruprasath, Control and Optimization of a Triple String Rotary Cement Kiln using Model Predictive Control, IFAC-Pap. 49 (2016) 748–753. https://doi.org/10.1016/j.ifacol.2016.03.146.
[149] V. Ramasamy, R. Kannan, G. Muralidharan, R.K. Sidharthan, R. Amirtharajan, Two-tier search space optimisation technique for tuning of explicit plant-model mismatch in model predictive controller for industrial cement kiln process, Math. Comput. Simul. 193 (2022) 385–408. https://doi.org/10.1016/j.matcom.2021.10.015.
[150] K.S. Stadler, J. Poland, E. Gallestey, Model predictive control of a rotary cement kiln, Control Eng. Pract. 19 (2011) 1–9. https://doi.org/10.1016/j.conengprac.2010.08.004.
[151] K.I. Janati, Thermo-elastic behavior study of rotary kilns for cement plants, Eng. Fail. Anal. 118 (2020) 104896.
[152] E. Alonso, A. Gallo, M.I. Roldán, C.A. Pérez-Rábago, E. Fuentealba, Use of rotary kilns for solar thermal applications: Review of developed studies and analysis of their potential, Sol. Energy. 144 (2017) 90–104. https://doi.org/10.1016/j.solener.2017.01.004.
[153] S. Tescari, P. Sundarraj, G. Moumin, J.P.R. Duarte, C. Agrafiotis, L. de Oliveira, C. Willsch, M. Roeb, C. Sattler, Solar rotary kiln for continuous treatment of particle material: Chemical experiments from micro to milli meter particle size, in: Daegu, South Korea, 2020: p. 140007. https://doi.org/10.1063/5.0029271.
[154] A. Meier, E. Bonaldi, G.M. Cella, W. Lipinski, D. Wuillemin, R. Palumbo, Design and experimental investigation of a horizontal rotary reactor for the solar thermal production of lime, Energy. 29 (2004) 811–821. https://doi.org/10.1016/S0360-5442(03)00187-7.
[155] S. Tescari, M. Neises, L. de Oliveira, M. Roeb, C. Sattler, P. Neveu, Thermal model for the optimization of a solar rotary kiln to be used as high temperature thermochemical reactor, Sol. Energy. 95 (2013) 279–289. https://doi.org/10.1016/j.solener.2013.06.021.
[156] A. Gallo, E. Alonso, C. Pérez-Rábago, E. Fuentealba, M.I. Roldán, A lab-scale rotary kiln for thermal treatment of particulate materials under high concentrated solar radiation: Experimental assessment and transient numerical modeling, Sol. Energy. 188 (2019) 1013–1030. https://doi.org/10.1016/j.solener.2019.07.006.
[157] M. Neises, S. Tescari, L. de Oliveira, M. Roeb, C. Sattler, B. Wong, Solar-heated rotary kiln for thermochemical energy storage, Sol. Energy. 86 (2012) 3040–3048. https://doi.org/10.1016/j.solener.2012.07.012.
[158] G. Moumin, S. Tescari, P. Sundarraj, L. de Oliveira, M. Roeb, C. Sattler, Solar treatment of cohesive particles in a directly irradiated rotary kiln, Sol. Energy. 182 (2019) 480–490. https://doi.org/10.1016/j.solener.2019.01.093.